國 立 交 通 大 學

電信工程學系

碩 士 論 文

似碎型左手超材質穿透特性之研究

Transmission Characteristics of Fractal-like Left-handed Metamaterials

研 究 生：陳慧文

指導教授：鍾世忠　教授

陳志隆　教授

中　華　民　國　九十四年六月

似碎型左手超材質穿透特性之研究

Transmission Characteristics of Fractal-like Left-handed Metamaterials

研 究 生：陳慧文　　Student：Hui-Wen Chen

指導教授：鍾世忠　　Advisor：Shyh-Jong Chung

陳志隆　　Jyh-Long Chern

國 立 交 通 大 學

電 信 工 程 學 系

碩 士 論 文

A Thesis

Submitted to Department of Communication Engineering

College of Electrical Engineering and Computer Science

National Chiao Tung University

in partial Fulfillment of the Requirements

for the Degree of

Master

in

Communication Engineering

June 2005

Hsinchu, Taiwan, Republic of China

中華民國九十四年六月

似碎型左手超材質穿透特性之研究

學生：陳慧文　　指導教授：鍾世忠

陳志隆

國立交通大學電信工程學系研究所碩士班

摘　　要

在左手超材質的研究議題上，最終的目標是將其應用到光波波段或者紅外波段。然而左手超材質其本身的特性將會使得在實行的過程上會有不可避免的困難點，尤其是製程和功率的問題。因此，在本篇論文中，我們試著去探討可能的解決方法。首先，一個同平面的結構將用來解決左手超材質以後在半導體製程上會遇到的問題。接著，我們提出兩種不同機制所產生之不同的耦共振結構，藉此希望能夠解決左手超材質本身長久以來存在的功率不足的問題。除此之外，我們也會對一些利用半導體製程所製作出來的左手超材質在紅外光波段進行探討與分析，以期能有關鍵性的突破。

Transmission Characteristics

of Fractal-like Left-handed Metamaterials

Student: Hui-Wen Chen Advisors: Dr. Jyh-Long Chern

Dr. Shyh-Jong Chung

Department of Communication Engineering

National Chiao Tung University

Abstract

On the path to create actual metamaterials within visible light region or infrared band, there are still some difficulties waiting to be overcome. Fabrication, power consumption and scale issue are parts of the numerous problems. In this thesis, we discover the solutions of the first two problems by experiment verification. A coplanar structure is first proposed for utilization in semiconductor fabrication issue. Another double resonant frequencies (DRF) pattern with two different mechanisms is used to meet the power topic. Some positive experiment results of DRF sample can provide sufficient information for further studies. In addition to the microwave observation, the metamaterials will be explored within infrared region in this thesis as well to supply direct evidence of optical response.

誌謝

非常感謝電信所的指導教授鍾世忠老師的寬大包容，讓我能夠有機會在光學的領域繼續鑽研。再來要感謝的是光電所的指導教授陳志隆老師，實驗室所提供的環境以及充足的資源，讓我無後顧之憂的進行研究。在過去的兩年之中，也謝謝老師給我許多自由的空間，讓我得以在研究之餘，能同時兼顧申請學校的種種事宜。還有工研院的蔡榮源組長、黎邦科長和曲昌盛先生的大力相助，沒有你們的協助，就沒有這本論文的誕生。

再來要感謝的是實驗室的各位學長姐，慈方、小利、小朱、介任、尹凱以及兆璽，謝謝你們在專業和生活上對我的啟發。在此我要特別感謝萓蓁，在我初到實驗室時提供許多專業上的知識以及協助。在生活上更是一個不可多得的好朋友，這個緣分我會永遠珍惜的。家佑、阿祥、晟傑和森年，我想我會永遠記得最後幾個月一起趕論文的甘苦的。最後要謝謝各位學弟妹，你們的加入為實驗室帶來了活力。

謝謝交大管樂團的大家，你們是我最好的朋友。這六年來的點點滴滴、酸甜苦辣以及一起經歷過的大小風雨，我都會銘記在心的。我只能說，少了你們，這六年將會是一片黑白。

謝謝冠中，你的愛心早餐讓我變胖不少。

感謝我的父母，希望你們能永遠健康平安。

Contents

List of Figures

List of Tables

Chapter 1

Introduction

Curiosity is the nature instinct that human beings have in whole life. Most great scientific development in history starts from a tiny curiosity that might be ignored. It is, in my belief, the curiosity of discovering and constructing novel negative index of refraction giving a birth to this thesis. The properties and applications of such a material especially inspire people's imagination and discussion due to lack of materials with negative refraction index in nature occurring substances. This innovative material, if it is successfully created, will bring extremely huge impact to modern optical system and physical vision. For instance, a convex lens with negative refraction index will make the incident light diverge from the lens rather than converge to a focal point. Moreover, phase and group velocity of electromagnetic waves could propagate in opposite directions so that the propagation direction is reversed with respect to the Poynting vector. This kind of discussion concerning negative index material can be expanded depending on people's invention.

In the past few years, some research groups in U.K. and U.S.A had built up fundamental knowledge and experiments to demonstrate the existence of negative refraction index at X-band; and presented the possibility of fulfilling such a material. However, the researches related to metamatrials which had been done are not yet completed. The space of improvement, such as depression of lattice constant, enhancement of loss, and fabrication techniques, are still accessible. Consequently, the efforts of this thesis, basing on previous research, concern about amending the

drawbacks of former experiments.

1.1 Brief Review of Metamaterials

The effects induced by the existence of negative permeability and permittivity had been explored so early by Veselago in 1968 [1]. Novel properties such as negative refraction index and reversed Doppler shift were proposed. Nevertheless, while negative permittivity can be obtained in the nature world under certain special condition (for instance, the effective permittivity possesses negative value below plasma frequency of metal), the negative permeability is still hard to exhibit (as shown in Fig. 1.1 [2]).

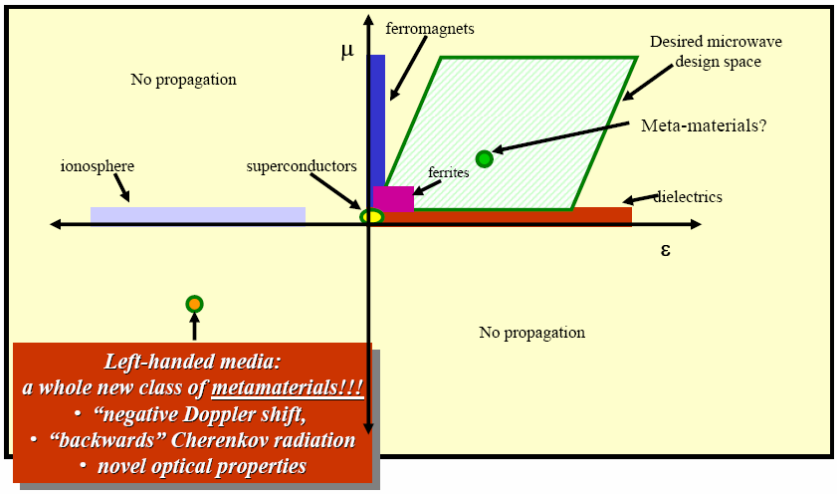

Figure 1.1: Permittivity and Permeability space of materials. Our purpose is to fulfill the void of the third quadrant [2].

The solution of negative permeability doesn't appear until Pendry *et al.* [3] proposed a metallic split ring resonator (SRR), to achieve this goal. The work has drawn a great attention of many people to complete. Soon after, Smith *et al.* reported the demonstration of left-handed metamaterials by combining the SRRs and periodical wires together [4][5]. This is a milestone in the progress of left-handed metamaterial, and those works also show the possibility of achieving some novel applications. For instance, the perfect lens, which is made by a slab of negative

refraction index material, has the power to focus the light at one point and thus can break the diffraction limit under certain conditions [5]. This is extremely useful in optical system design and other optical fields.

In 2004, our group proposed a novel structure called deformed SRR (DSRR), and successfully demonstrated the property of negative permeability with smaller lattice constant [10][11]. Such an innovation pattern with slightly difference from SRR can still possess similar electromagnetic response as well, but reduces the lattice constant and volume by 40%. In addition to decrease the lattice constant of cells, our group also developed another practical structure named smile pattern resonator (SPR) to widen the bandwitdth of absorption band [17]. Considering further realistic applications, the pattern with wider absorption spectrum can increase the diversity of this field; each case needs different ring structure to achieve its own requirement. Moreover, an experiment with a slab of negative refraction-index is demonstrated to break the limitation of diffraction [18].

Nowadays, the research related to metamaterials is still under investigation. More and more research groups and resources had been invested in this area. The benefits with this inventive material will be enormous. In the next five to ten years, it will be the crucial period for the development of metamaterials. In conclusion, there are still numerous topics in this area to be discovered for the next decade.

1.2 Motivation

Groups of Pendry and Smith had established basic knowledge in this area. However, there are still a lot of works that we can modify from prior results. First of all, the structure of composite metamaterials with SRRs and wires lying on the opposite plane of the printed circuit board will encounter difficulties while the scale goes down to nanometer level. A pattern with structures on both planes is not allowed in semiconductor process. Hence a coplanar structure might be useful in future application. Next, the loss of metamaterials in GHz range is quite large comparing to commercial microwave devices. This disadvantage might impede the further application of metamaterials since efficiency is a very important factor in all systems. Therefore, how to raise the power level of the electromagnetic wave after passing

metamaterials should be a main concern in future development. The most important of all, our final destination is to implement metamaterials in visible range, say, in optical system. Hence the optical response of nano-scale pattern will be discovered. Negative refraction index will impact modern optics and bring some new idea to the concept of optical system design. According to the restriction that the lattice constant should be much smaller than operating wavelength, technology of fabricating metamaterials would be a challenge in semiconductor process. There will be various applications if the work can be realized in visible range. In conclusion, my motivation is to improve the efficiency and performance of previous results; eventually to achieve negative refraction index in visible region.

1.3 Organization of This Thesis

The organization would be mainly divided into six parts in this thesis. Besides basic theory of metamaterials described in Chapter 2, the following chapters will be introduced the detail about my research. Three topics concerning the improvement will be presented in Chapter 3 , Chapter 4 and Chapter 5. A new structure with SRRs and wires locating on the same plane will be discussed in Chapter 3. In Chapter 4, the idea of double resonant frequency is proposed while trying to compensate the loss of metamaterials. An additional chapter showing some experiment results of metamaterials at 1550nm infrared region will be discovered and analyzed in Chapter 5. Finally, the conclusion and some future works will be included in Chapter 6.

Chapter 2

Basic Theory of Left-Handed Materials

Veselago, in a paper published in 1968 [1], pondered the consequences for electromagnetic waves interacting with a hypothetical material for which both the electrical permittivity ε and the magnetic permeability μ were simultaneously negative. Because negative permittivity and permeability have not ever been demonstrated to exist in natural materials or compounds, Veselago wondered whether this material was just a fantasy or perhaps had a more fundamental origin. He concluded that not only should this material be possible, but if ever found, it would exhibit remarkable properties unlike any other known materials and bring huge impact to all electromagnetic phenomena.

Since the vectors $\vec{E}$, $\vec{H}$, and $\vec{k}$ of a plane wave in such material form a left-haneded set, Veselago referred to the material as left-handed materials (LHMs). This material is also called negative refraction index material or metamaterials due to the negative property revealing in it.

Veselago's concept was not realized until 1996, while Pendry purposed a periodic thin wire structure which exhibits negative permittivity below the plasma frequency [6]. Three years later, a nonmagnetic split ring resonator (SRR) performing negative permeability below the magnetic plasma frequency was discovered by Pendry [3]. In 2001, Smith combined periodic wires and SRR structure, and successfully demonstrated the phenomena of negative refraction by measuring the

refraction angle of composite LHMs which gave the evidence of negative refraction index [4]. Since then, the research related to LHMs has inspired great interest. In this chapter, we will review the fundamental electromagnetic theory and experimental demonstration of LHMs.

2.1 Veselago's Idea

To understand Veselago's idea, we have to start from Maxewell equation and the constitutive relations first.

$$\nabla \times \vec{E} = -\frac{\partial \vec{B}}{\partial t}$$
$$\nabla \times \vec{H} = \vec{J} + \frac{\partial \vec{D}}{\partial t} \tag{2.1}$$

$$\vec{D} = \varepsilon \vec{E}$$
$$\vec{B} = \mu \vec{H} \tag{2.2}$$

For a monochromatic plane wave with the form of $e^{i(\vec{k}\cdot\vec{r}-\omega t)}$, we can rewrite Eq.2.1 and 2.2 as following :

$$\vec{k} \times \vec{E} = \omega \mu \vec{H}$$
$$\vec{k} \times \vec{H} = -\omega \varepsilon \vec{E} \tag{2.3}$$

It can be understood clearly from the equation that if both permittivity and permeability are positive, the vectors $\vec{E}$, $\vec{H}$, and $\vec{k}$ form a right-handed set. On the contrary, if the sign of permittivity ε and permeability μ changes from positive to negative, then $\vec{E}$, $\vec{H}$, and $\vec{k}$ will establish a left-handed triplet of vectors. In this condition, Eq.2.3 can be modified as:

$$\vec{k} \times \vec{E} = -\omega |\mu| \vec{H}$$
$$\vec{k} \times \vec{H} = \omega |\varepsilon| \vec{E} \tag{2.4}$$

As for the Poynting Vector,

$$\vec{S} = \vec{E} \times \vec{H} \tag{2.5}$$

which is only related to electrical and magnetic fields, it can also be described in the left-handed concept. Fig. 2.1 (a) displays the relation of Eq.2.5 in a conventional

medium where energy flux $\vec{S}$ is parallel to the wave vector while phase and group velocity coincide with each other.

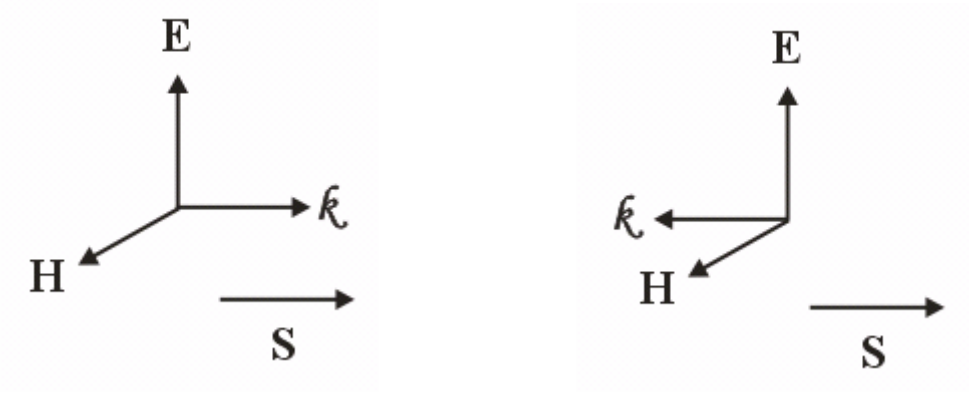

(a) (b)

Figure 2.1: Poynting vector in right-handed and left-handed media

In LHMs, however, the Poynting vector is anti-parallel to the wave vector which shows that the phase and group velocity are in opposite directions. In other words, the term of LHMs is equivalent to the term "material with negative group velocity." Meanwhile, since the energy flux $\vec{S}$ is opposite to the phase velocity, the wave front would move toward energy source and is opposite to the propagating direction. Hence some phenomena such as Doppler effect and Vavilov-Cerenkov effect will be reversed.

Now, let us consider the consequence that will happen on the interface between LHM and RHM. First, the boundary condition of electromagnetic wave must be considered. According to Eq.2.5, the tangential component of E and H are unaffected. However, the normal components of $\vec{E}$ and $\vec{H}$, with $\varepsilon < 0$ and $\mu < 0$, will undergo a change of sign at the interface between a RHMs and a LHMs as shown in Fig. 2.2.

$$\begin{aligned} E_{t_1} &= E_{t_2} \\ H_{t_1} &= H_{t_2} \\ \varepsilon_1 E_{n_1} &= \varepsilon_2 E_{n_2} \\ \mu_1 H_{n_1} &= \mu_2 H_{n_2} \end{aligned} \tag{2.5}$$

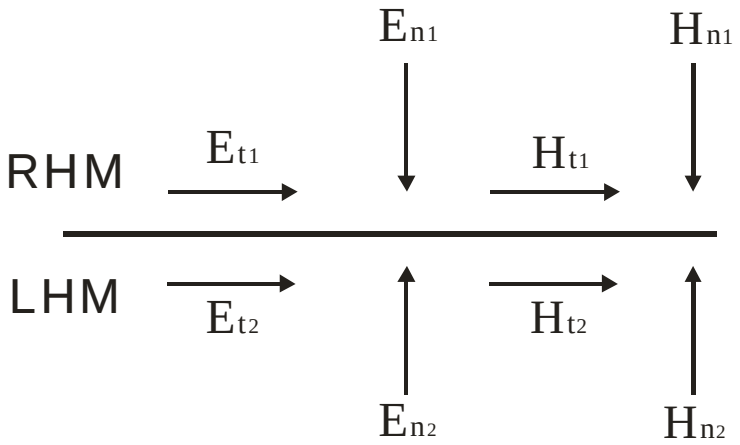

Figure 2.2: Boundary condition at the interface between a RHM and a LHM.

Since the relation between RHMs and LHMs is different from conventional condition, Snell's Law can be modified in a special view. That is, while the wave transmitting through the boundary of RHMs and LHMs, it will introduce a negative refraction angle which can lead to a negative refraction index in the LHMs according to Snell's Law : $n_1 \sin\theta_1 = n_2 \sin\theta_2$.

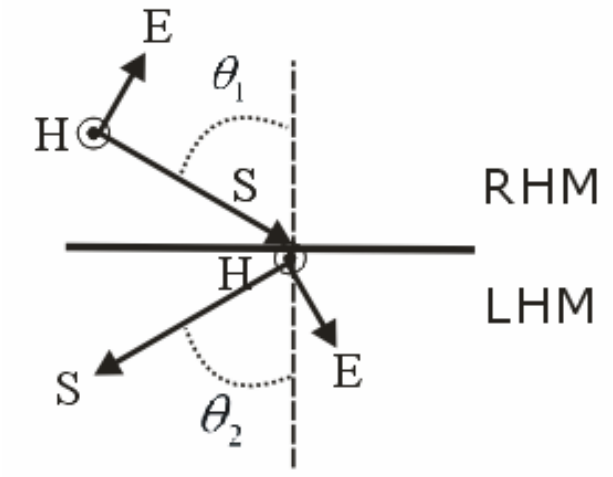

Figure 2.3: The refraction angle showing the property of LHM.

Furthermore, the mathematic calculation of $n = \sqrt{\varepsilon\,\mu}$ is another explanation to derive negative refraction index in LHMs. It should be more careful in taking the square root because ε and μ are analytic functions whose values are generally complex. There is an ambiguity in the sign of the square root that is solved by a

proper analysis. Hence, by taking $\sqrt{\varepsilon} = i\sqrt{|\varepsilon|}$ and $\sqrt{\mu} = i\sqrt{|\mu|}$, we can get a negative sign for n in LHMs. The step of taking the square root of either ε or μ alone must have a positive imaginary part is a necessary one for passive material.

In summary, the negative refraction index comes from the combination of negative permittivity and negative permeability. Special phenomena, such as negative refraction angle, reverse Doppler effect and revised boundary condition, can be predicted basing on the derivation. Practical implementation of negative permittivity and negative permeability will be elucidated in next two sections.

2.2 Wire Structure of Negative Permittivity

In this section, the effect of metallic thin wires which exhibit plasma frequency in low frequency, say, GHz range will be introduced. Theoretical derivation and examples will give a physical vision to thin metallic wires. The point of "thin" wires is extremely crucial because thick wires would not reach the same function of negative permittivity.

In our knowledge, metals in the visible region and ultraviolet display a plasmon which is a collective oscillation of electron density. The charge on the electron gas is compensated by the background nuclear charge in the state of equilibrium. Under the effect of electromagnetic force, the negative electron gas and a surplus of uncompensated charge are generated at the ends of the specimen. This supply a restoring force between the opposite charges following a simple harmonic motion,

$$\omega_p{}^2 = \frac{de^2}{\varepsilon_0 m_{eff}} \tag{2.6}$$

where *e* is the electron charge, *d* is the density of electrons, and m_{eff} is the effective mass of electrons. With the interaction with electromagnetic radiation, the plasmon produces a dielectric function of the form,

$$\varepsilon(\omega) = 1 - \frac{\omega_p{}^2}{\omega(\omega + i\gamma)} \tag{2.7}$$

where γ is the damping factor representing dissipation of the plasmon's energy into the system. Meanwhile, it is small relative to ω_p.

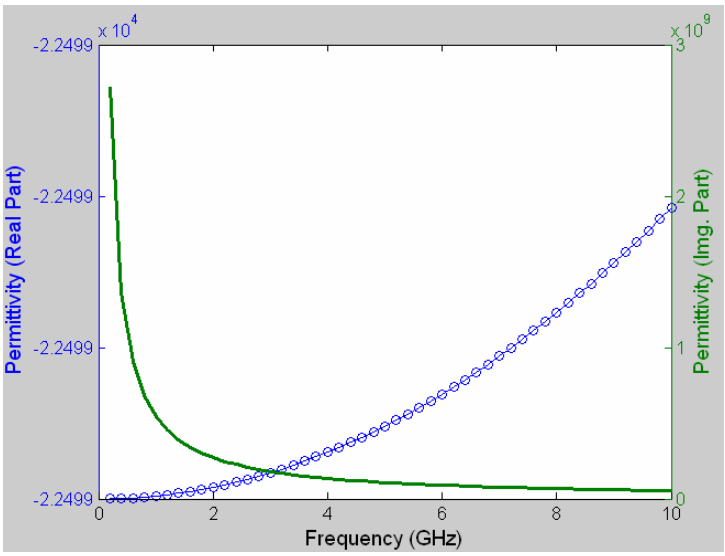

Figure 2.4: Dielectric function at lower frequency shows the domination of imaginary part. The real part is marked by clear circles while imaginary part is labeled by solid line.

Nevertheless, Eq.2.6 will become imaginary in the GHz frequency range because of the inevitable dissipation. As shown in Fig. 2.4, the imaginary part of permittivity is much lager than the real part. In other words, the dielectric function at lower frequency is dominated by the imaginary part, which is exactly out of our expectation. Hence, a composite material that translates the characteristic feature of metallic response at ultraviolet region into GHz range is desirable

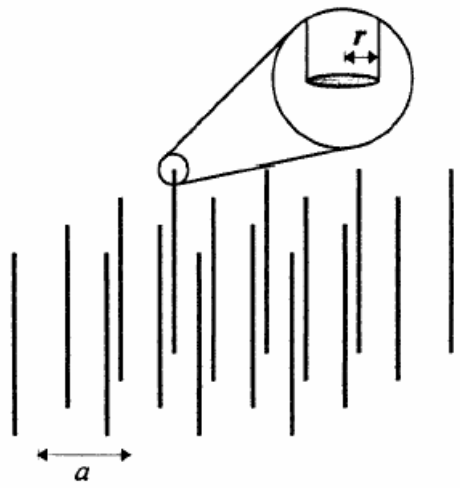

Figure 2.5: An array of infinite wires aligned with the *z* axis and arranged on a square lattice in the x-y plane. In the structure we considered, *a* might be a few millimeters and *r* a few microns [8].

In 1996, Perndry *et al.* [6] proposed a composite structure built by metallic thin wires which depressed the plasma frequency to GHz range. As shown in Fig. 2.5, thin metallic wires will confine the motion of electrons, then changing the effective mass of them. Because only part of the space is filled by metal, the average electron density is reduced to

$$d_{eff} = d\frac{\pi r^2}{a^2} \tag{2.8}$$

Another factor we have to consider is an enhancement of the effective mass of the electrons caused by magnetic effects. This self-inductance gives an additional contribution to the momentum of $e\mathbf{A}$, and therefore the new effective mass of electrons is given by

$$m_{eff} = \frac{\mu_0 e^2 \pi r^2 d}{2\pi} \ln(a/r) \tag{2.9}$$

With the enormously enhanced effective mass and decreasing electron density, the plasma frequency will shift from ultraviolet region to GHz range, which is a correspondingly large amount. A sample of actual calculation will give below.

Example: aluminum wires

$r = 1.0\times10^{-6}$ m $\qquad a = 5$ mm

$d = 1.806\times10^{29}$ m^{-3} (aluminium)

$\Rightarrow \quad m_{eff} = 2.7233\times10^{4} m_e$, much larger than electron mass

$\Rightarrow \quad \omega_p = 8.20$ GHz

Form this mathematic work, a clear view of our composite metallic thin wires can be seen. The structure successfully decreases the plasmon frequency in a huge amount; hence the negative permittivity in microwave range is available. After solving the requirement of negative permittivity, the possibility of negative permeability will be discussed.

2.3 Ring structure of negative permeability

In the above section, the wire structure which conceptually replaces the atoms and molecules of a real material and presents negative permittivity property is introduced. Although naturally occurring magnetic monopoles do not exit, a structure utilizing the concept of Drude-Lorentz model can bring negative permeability into reality. In 1999, Pendry *et al.* proposed a microstructure mimicking ordinary uniform material, and successfully showed the negative permeability [3].

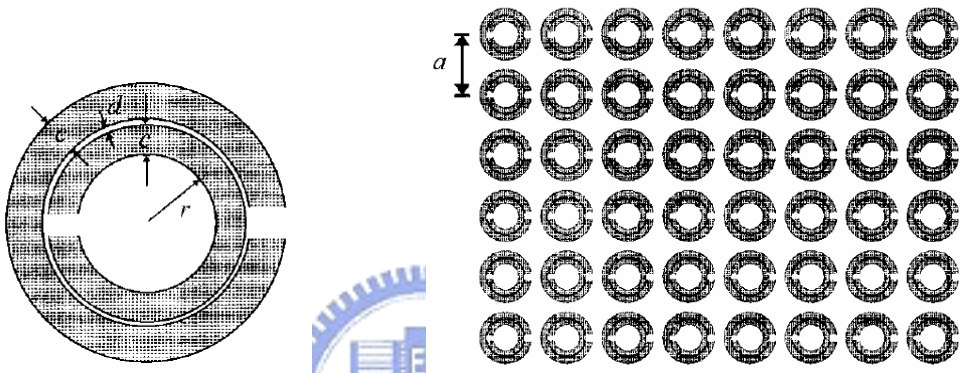

(a) (b)

Figure 2.6: (a) Schematic layout of a single split ring resonator (SRR). A SRR has two conductive loops with a gap inserted. There is a small space between two loops, which can produce inner capacity. (b) The composite media of SRR array. The lattice constant *a*, which is about one tenth of the wavelength, is a crucial factor of this media [3].

As shown in Fig. 2.6, this structure consists of split ring resonator (SRR) array where *r* is the radius of the inner split ring of each SRR, *c* is width of each ring, and *d* is space between two split rings. Each SRR which behaves like an atom or a molecule has two conductive loops with a gap inserted. This gap prevents current from following around any one ring. However, there is a considerable capacitance between the two rings, which enable current to flow. The greater the capacitance between the two loop, the larger the current induced. The capacitance between different SRRs, moreover, must be considered in our calculation. Sequentially, the self-inductance of large capacity in and between the SRRs, which cause electrical

current following in two separating loops, will play the role of magnetic dipole. In this case, the permeability will satisfy

$$\mu_{eff} = 1 - \frac{F\omega^2}{\omega^2 - \omega_0{}^2 + i\omega\Gamma} \tag{2.10}$$

where $F = \frac{\pi r^2}{a^2}$ is the filling factor which represents the fractal area occupied by SRRS of each unit cell, $\Gamma = \frac{2l\rho}{r\mu_0}$ is the dissipation factor, and

$$\omega_0{}^2 = \frac{3lc_0{}^2}{\pi r^3 \ln(\frac{2c}{d})} \tag{2.11}$$

is the frequency where μ_{eff} diverges or resonant frequency. The symbol l is the distance between two layers, ρ is the resistance of unit length of the sheets measured around the circumference, and c_0 is the light velocity in vacuum. While a perfect conductivity material is used, the term of dissipation will vanish as well; hence Eq.2.6 can be modified as

$$\mu_{eff} = (1-F)\frac{\omega^2 - \omega_{mp}{}^2}{\omega^2 - \omega_0{}^2}, \quad \text{where } \omega_{mp}{}^2 = \frac{\omega_0{}^2}{1-F} \tag{2.12}$$

ω_{mp} is the magnetic plasma frequency. The relation of effective permeability, ω_{mp}, and ω_0 is shown in Fig. 2.7. The region from ω_0 to ω_{mp} is what we desired for this micro-scale structure.

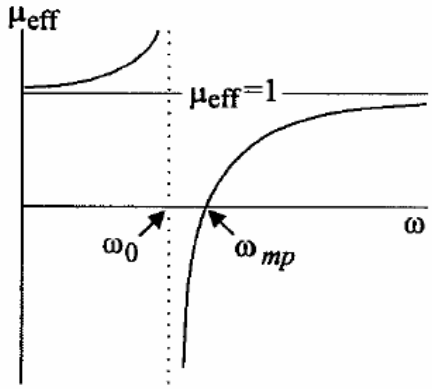

Figure 2.7: Typical curve showing the effective permeability of SRR array. Permeability locating in the region between ω_0 and ω_{mp} exhibits expected negative value [3].

For SRR with parameter a = 10 mm, c = 1 mm, d = 0.1 mm, l = 2 mm, and r = 2 mm, the estimated resonant frequency will be

$$\omega_0^{\,2} = 7.1\times10^{21}$$

$$\Rightarrow \quad f_0 = 13.5\,\text{GHz}, \quad f_{mp} = 14.4\,\text{GHz}$$

Consequently, negative permeability can be realized in microwave range. The band desired in our calculation is pretty narrow, say, about 10%. In the forbidden band, a propagating plane wave in this composite SRR media will attenuate smoothly and eventually vanish because of the imaginary term in wave factor, say, $k = n \cdot k_0 = i\sqrt{|\varepsilon||\mu|} \cdot k_0$ in $e^{i(\vec{k}\cdot\vec{r}-\omega t)}$. In other words, the transmission power of electromagnetic wave after passing through a SRR media is barely detectable. Thus, as shown in Fig. 2.8, a band-stop like characteristic in X-band spectrum is the classic curve of a SRR media.

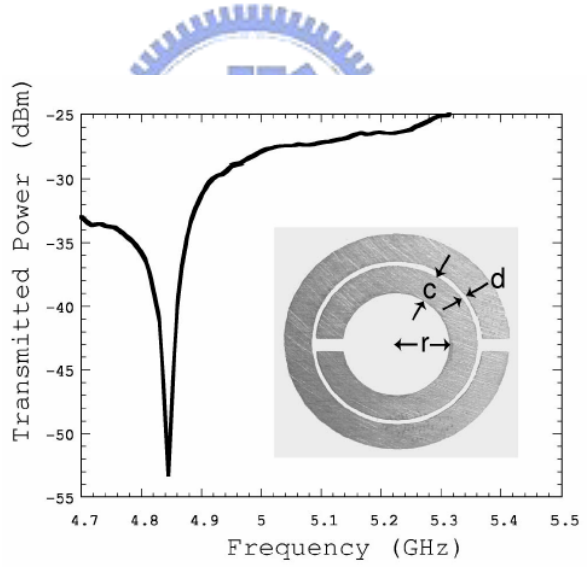

Figure 2.8: Transmission spectrum showing the characteristic of a single SRR. The band-stop like behavior is due to the negative permeability caused by SRR structure [9].

2.4 Experimental Demonstration of LHMs

In the above two sections, the accomplishments of negative permittivity and negative permeability are described in detail. However, the demonstration of negative refraction index is still not available. Although the materials of both negative permittivity and negative

permeability are separating obtained, we are not sure if the combination of periodic wires and SRRs will work successfully. Will unpredicted interaction between wires and SRRs destroy the behavior of their own?

In 2000, Smith *et al.* presented the numerical simulation and experimental data to prove simultaneously negative permittivity and permeability effect. He fabricated the SRRs and wires on commercial available printed circuit board [9]. In his experiment, square arrays of SRRs and wires were constructed with a lattice spacing of 8 mm between elements. The result of transmission experiments on SRRs alone (solid curve), and SRRs with wires (dashed curve) are shown in Fig. 2.9.

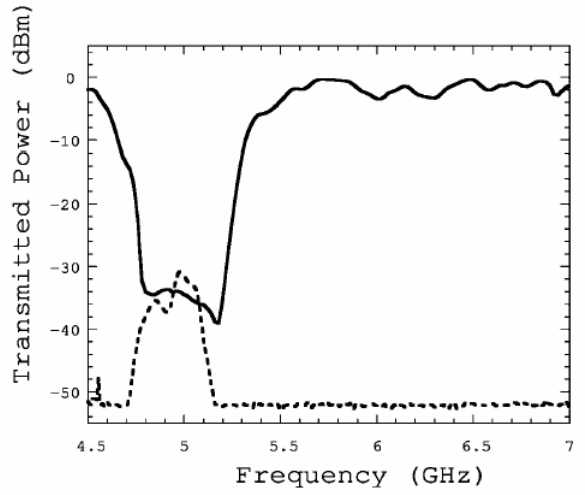

Figure 2.9: Experimental result for LHMs. Solid line is the transmission spectrum of SRRs alone while dashed line is the transmission curve of SRRs with wires. A pass band of LHMs about 5 GHz is observed [9].

Following the conclusion that we have made in Sec.2.3, the transmission power will attenuate between f_0 and f_{mp} as the solid curve shown. However, while SRRs are united with periodic wires, a negative refraction index will be obtained by simultaneous negative permittivity and permeability. The wave which originally attenuates will thus propagate due to a real wave factor (from $i\sqrt{|\varepsilon||\mu|}\cdot k_0$ to $-\sqrt{|\varepsilon||\mu|}\cdot k_0$). On the other hand, the wave which originally propagate (for instance, above 5.5 GHz) will thus become attenuating wave according to imaginary wave factor as well. Therefore, the transmission power locating on the absorption band previously exhibit a pass band characteristic basing on effect of negative

refraction index.

Although the demonstration of the composite LHMs has been completed, a more directly evidence of negative refraction index is still unavailable. We need a straightforward experiment result to convince everyone the existence of negative refraction index.

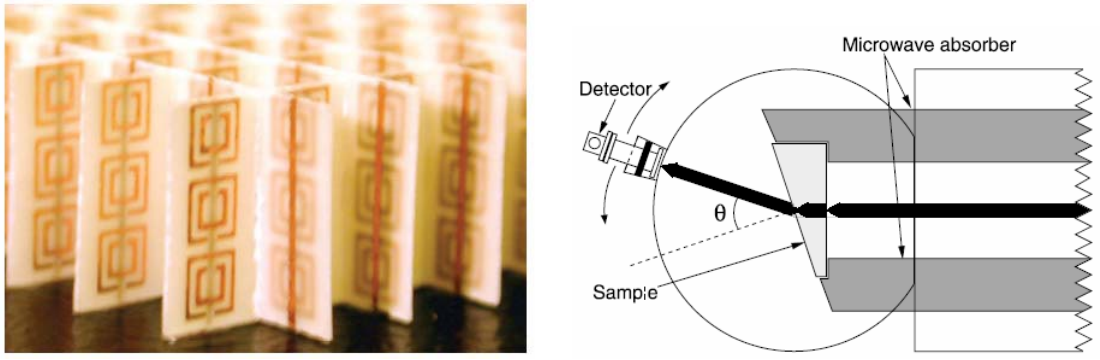

(a) (b)

Figure 2.10: (a) Photograph of the LHM sample. It consists of square copper SRRs and wire strips on glass circuit board. The rings and wires are on opposite sides of the boards. (b) Diagram of experimental setup. The black arrows represent the microwave beam as would be refracted by a positive index sample [4].

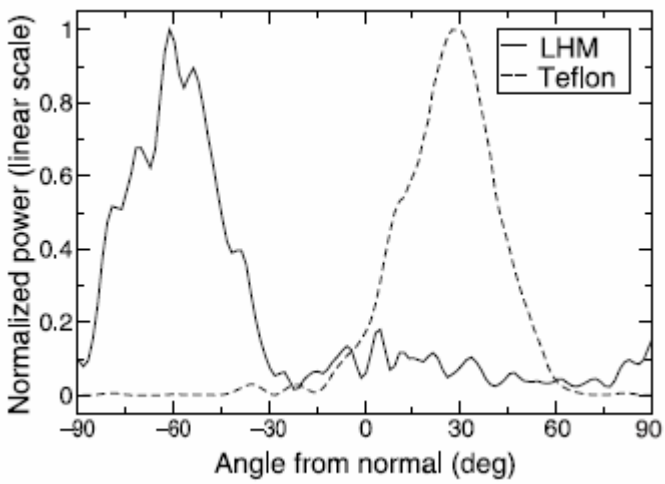

Figure 2.11: Experimental data of measuring refractive angle of LHM and Teflon. The positive degree of Teflon provides the reference for LHM while the negative degree offers the evidence of negative refraction index [4].

In 2001, Smith *et al.* performed and experiment of Snell's Law with a wedge composed of the LHMs (Fig. 2.10) [4]. By measuring the scattering angle after microwave beam transmitting the wedge, the effective refraction index can be determined. The refractive power peak of Telfon should be positive degree, as shown in Fig. 2.11, corresponding to positive refraction index. However, the power peak of microwave after passing through the LHM wedge locates at -61 degree, from which we deduce the index of refraction to be -27 ± 0.1. Hence, the measurement successfully demonstrates the existence of negative refraction index at first time.

Chapter 3

Coplanar Structure of Metamaterials

The concept of negative permeability at certain frequency caused by SRRs is most interesting because the resonant frequency has strong relation with unit length and lattice constant. Recently, deformed SRR (DSRR) [10] [11] has provided a practical way to decrease the size of lattice constant, which is very useful while the short wavelength electromagnetic wave propagating in LHMs is desired.

Figure 3.1: A single DSRR with the property which can increase the resonant frequency with the same lattice constant as SRR.

When it comes to optical region, DSRRs whose scale is only about nanometers can be manufactured through the semiconductor process. However, there is still another problem companied by semiconductor process although it provides a practical method of such a small scale. Semiconductor process has a limitation that the metallic patterns can only be placed on a single plane, which means the wires and

DSRRs must be fabricated separately. In such a small scale, the orientation between wires and resonant rings will be a difficult problem and is hard to solve. Hence, we need a novel metallic structure, which consists of coplanar wires and resonant rings altogether in order to avoid those inconvenient factors in semiconductor process.

3.1 Design for Coplanar Structure of Metamaterials

As our knowledge, the construction of metamaterials has two parts. One is the ring structure which presents the negative permeability, and the other is the periodic wire which presents the negative permittivity. Hence, the design for coplanar structure must be divided into two parts – negative permeability and negative permittivity. That is, we have to modify the original SRRs and wires; and combine them at the same plane. In the next two subsections, a symmetric DSRR will be introduced to give the possibility of coplanar structure. Because the lattice constant of such a symmetric DSRR is twice as the original DSRR, the wire structure with the same lattice constant may not exhibit negative permittivity at resonant frequency. Therefore, discontinuous wires with different length must be considered in order to compensate the insufficiency.

3.1.1 Symmetric DSRR

In order to place the wire structure in the middle of ring structure, previous SRRs or DSRRs structures need to be modified. For SRRs, it is impossible to put metallic wires in the middle of them since they will cause inevitable contact with each other. Such contact will finally bring unpredicted phenomenon that would destruct our desired efforts. On the contrary, DSRRs, which is distinct from SRRs, is possible to place metallic wires in the center of the rings. The gap between the two halves of each DSRR provides the possibility to build a coplanar structure. The most direct way to implement such a coplanar structure is to rotate DSRRs by 45 degree and redistributed the two parts of one DSRR equally.

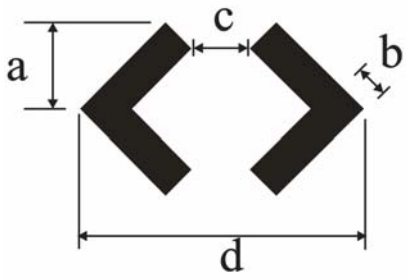

Figure 3.2: Schematic diagram of a single symmetric DSRR where a = 1.531 mm, b = 0.655mm, c = 1.000 mm, and d = 4.988 mm.

As Fig. 3.2 shown, a modified DSRR called symmetric DSRR is presented. The gap c allows the existence of metallic wire without any contact; hence the functions of rings and wires can perform separately. Meanwhile, the total unit length of this symmetric DSRR increases from 2.62 mm to 4.988 mm, which indicates that the original lattice constant, 5mm, is not suitable anymore. A wider lattice constant is necessary for this symmetric DSRR. In our concern, default lattice constant is set to be 10 mm which is twice the length of original DSRR.

3.1.2 Variation of Wire Length

After solving the negative permeability structure by proposing a model of symmetric DSRRs in the above subsection, we have to continue our article on negative permittivity of periodic wires. As mentioned before, the plasma cutoff frequency is strong related to wire width and lattice constant. Here, by changing angular frequency to frequency and replacing Eq.2.8 and 2.9 into Eq.2.6 and 2.7, the cutoff plasma frequency and dielectric function will be

$$f_p^{\,2} = \frac{c_{light}^{\,2}}{2\pi a^2 \ln(a/r)} \tag{3.1}$$

$$\varepsilon(f) = 1 - \frac{f_p^{\,2}}{f^2 + 2i\gamma' f} \tag{3.2}$$

where $\gamma' = \frac{\gamma}{4\pi} = \frac{\varepsilon_0 a^2 f_p^{\,2}}{r^2 \sigma}$ and σ is the conductivity. To match the lattice constant of symmetric DSRRs, the lattice constant of periodic wires should also be 10 mm.

However, the cutoff plasma frequency will be far below desired operating frequency while possessing such lattice constant.

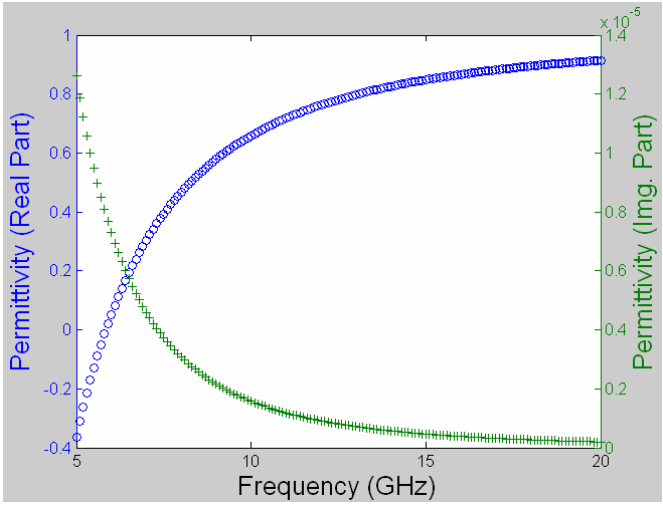

Figure 3.3: The relation of frequency and permittivity. Circle sign presents the real part of permittivity and plus sign presents the imaginary part of permittivity. The cutoff plasma frequency will locate at 5.84GHz while the lattice constant is 10 mm, the wire radius is 0.15 mm, and the conductivity of copper is 5.8×10^{7} S/m.

A more mathematical example is given for further acknowledge. Here copper is chosen as the fabricating material and wire radius is set to 0.15 mm. The estimated cutoff plasma frequency will be about 5.84GHz by calculating through Eq.3.1 and 3.2. In other words, the metallic wires will not behave like negative permittivity structure at desired resonant frequency from 10GHz to 20GHz just as shown is Fig. 3.3. From calculation above, permittivity of continuous metallic periodic wires is proved to take positive value at resonant frequency; hence another structure with negative permittivity trait is necessary. Fortunately, the discontinuous wire structure provides a choice other than continuous one. For cut wire structures, the negative permittivity region does not extend to zero frequency, and there appears a stop band around the resonant frequency [12]. The work accomplished by Ozbay shows that with the same wire radius, discontinuous wire structure can present negative permittivity from about 7 to 17 GHz while its plasma frequency being 7.39 GHz. In other words,

discontinuous wires can behave like negative permittivity medium just above the plasma frequency with the same wire radius of continuous one. Hence this kind of discontinuous wire can be inserted in the middle of symmetric DSRRs and give the negative permittivity property as expect.

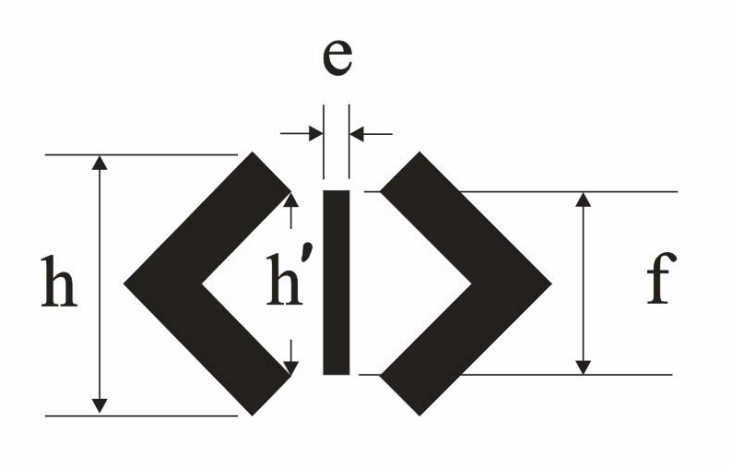

Figure 3.4: The schematic diagram of a single coplanar unit with shortest wire length. The wire width *e* is equal to 0.300 mm, *h’* = 2.135 mm, and *h* = 30.62 mm. The length of wire would is set to four values which is 2.135 mm, 2.444mm, 2.753mm, and 9.185mm.

When adding the discontinuous wires into symmetric DSRRs, the relative position between wires and symmetric DSRRs must be concerned carefully. Here four different sizes of wire length are chosen as shown in Fig. 3.4. The wire length will vary from 2.135mm to 9.185mm. First, the length of wire1 equal to the inner length of symmetric DSRRs is chosen. Wire2 exceeds the inner boundary by 1/3 difference between the inner and outer length of a single symmetric DSRRs while wire3 exceeds that by 2/3 length. Finally, wire4 with similarity to continuous wire is presented. The relation between different wires and symmetric DSRRs is awaited to discover, and the final destination is to build up a coplanar structure for metamaterials.

3.1.3 Specification of Coplanar Structure

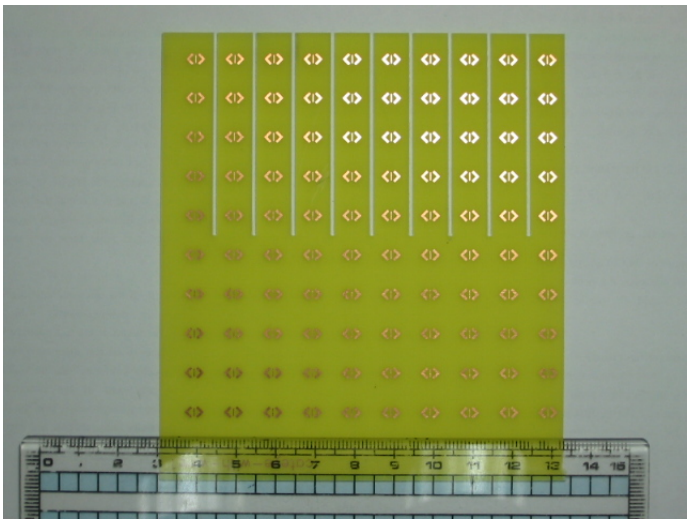

Figure 3.5: Overview of a single PCB with symmetric DSRRs and wire1 on it. The lattice constant is 10mm, and the total number of cells on per PCB is 100.

In experiment, four different types of a coplanar unit are measured. Separate symmetric DSRRs and various wires alone are also measured for the comparison. The lattice constant of each coplanar unit is set to be 10mm. The metallic medium that consists of periodical arrangement of wires and symmetric DSRRs is fabricated on a printed circuit board (PCB), which is transparent at X-band and 1mm thick. The total number of units on per PCB is 100 (10 cells in one row and 10 cells in one column).

3.2 Experiment Verification

After clearly definition of our coplanar pattern, the next step is to set up the experiment environment and get the actual experimental data to prove the above proposal. In this subsection, the experiment setup will be introduced first; following is the experiment results of coplanar samples.

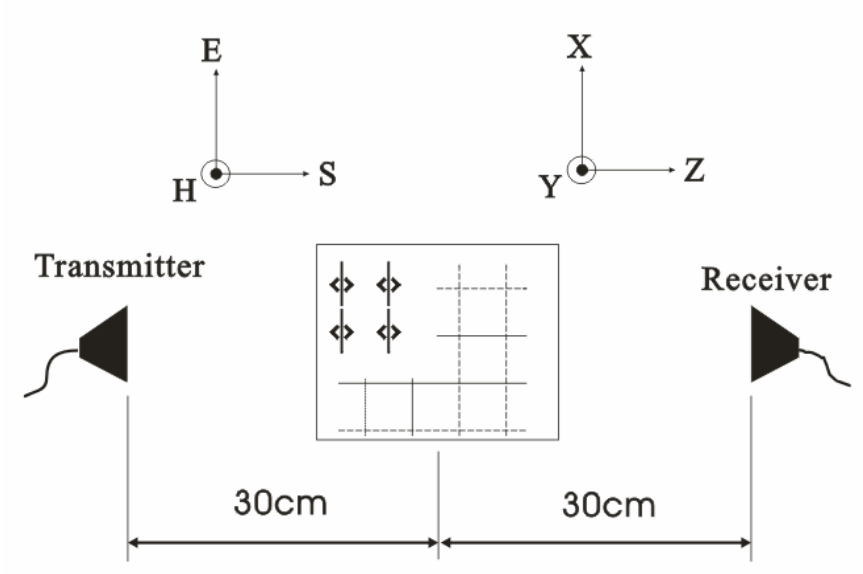

(a)

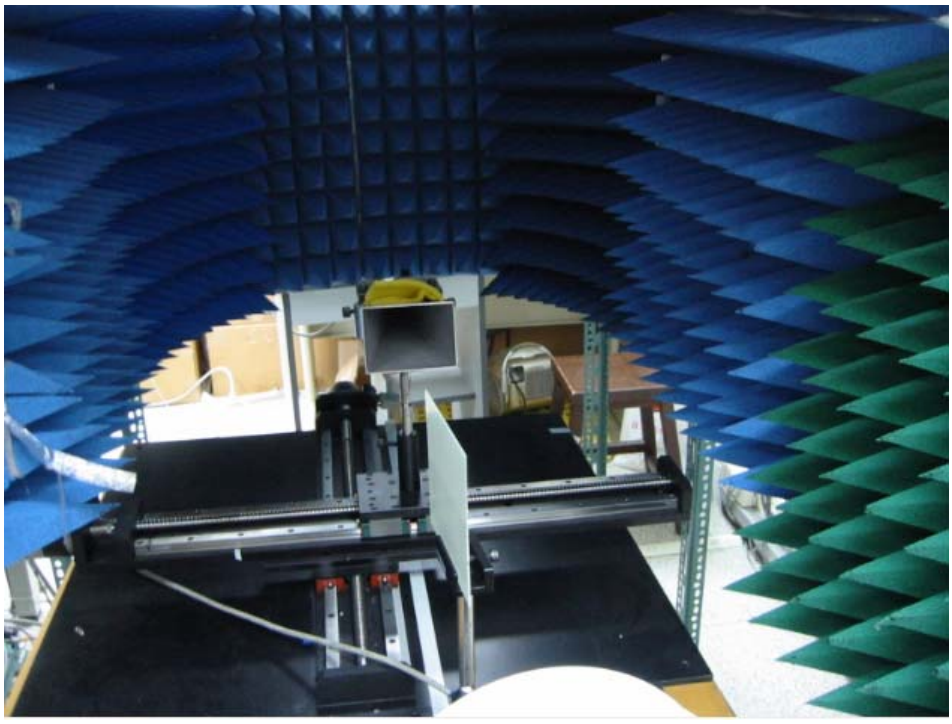

(b)

Figure 3.6: (a) Simple schematic diagram of experimental setup where the microwave is propagating along z axis and the sample is parallel to x-z plane. E and H indicate electric and magnetic field respectively. Both of the transmitter and receiver are 30cm from the center of the sample to avoid near field effects. (b) Photograph of experiment setup.

3.2.1 Experiment Setup

In experiment, a lens horn antenna (FLANN, 16810FA / 18094-SF40; operating frequency range is from 13.75GHz to 17.5GHz) is used as the transmitter to produce a time-varying linear electric field along ***x*** axis as the propagating direction is collimated with ***z*** axis as shown in Fig. 3.6. Hence, the magnetic field polarization is kept parallel to ***y*** axis. A standard gain horn (FLANN, 17240-20 / 17094-SF40; operating frequency range is from 9.84 to 15 GHz) is used as the microwave receiver in this experiment; both of the transmitter and receiver locate 30cm from the center of the sample. An Agilent Network Analyzer 8720D, whose frequency range is from 0.05GHz to 20.05GHz, is used to examine and record the response of the materials to the applied microwaves. Moreover, the whole experimental system is placed in a chamber consisted of microwave absorbers in order to prevent unpredicted reflection and interference waves during the measurements.

3.2.2 Experiment Results

In all experiment, the angle is set to be 0 degree while a single PCB is perpendicular to the ***x-z*** plane. In other words, the angle is set to be 90 degree while the PCB is parallel to the ***x-z*** plane. The S parameter is measured during the experiment process.

Symmetric DSRRs

The measured transmission characteristic of symmetric DSRRs is displayed in Fig. 3.7. A solid line indicates the response of the 0 degree symmetric DSRRs while clear rectangles present the response of the 70 degree symmetric DSRRs. The difference between 0 degree and 70 degree is not very obvious. However, as the PCB rotates to 80 degree, an apparent absorption which shows the angle sensitivity of symmetric DSRRs is observed. Next, we want to discuss about the results of symmetric DSRRs at 90 degree. The absorption spectrum which is denoted by solid circles, indicates that symmetric DSRRs has a power drop about 34.41dB comparing to 0 degree incident at the resonant frequency around 14.416 GHz..

Pendry *et al.* proposed that the lattice constant must be one tenth of the resonant

wavelength. In our experiment, however, the lattice constant of DSRRs is only about half of the wavelength. In fact, the resonant frequency is relative to the total number of cells; a slight difference of cell numbers will make the resonant frequency shift. In other words, as the cell number decreases, the resonant frequency will move toward higher part of spectrum. Furthermore, the unit length *d* is approximately one fourth of the wavelength which is also quite large comparing to the wavelength. Now, what we are interested in is the composite behavior of symmetric DSRRs and diverse wires.

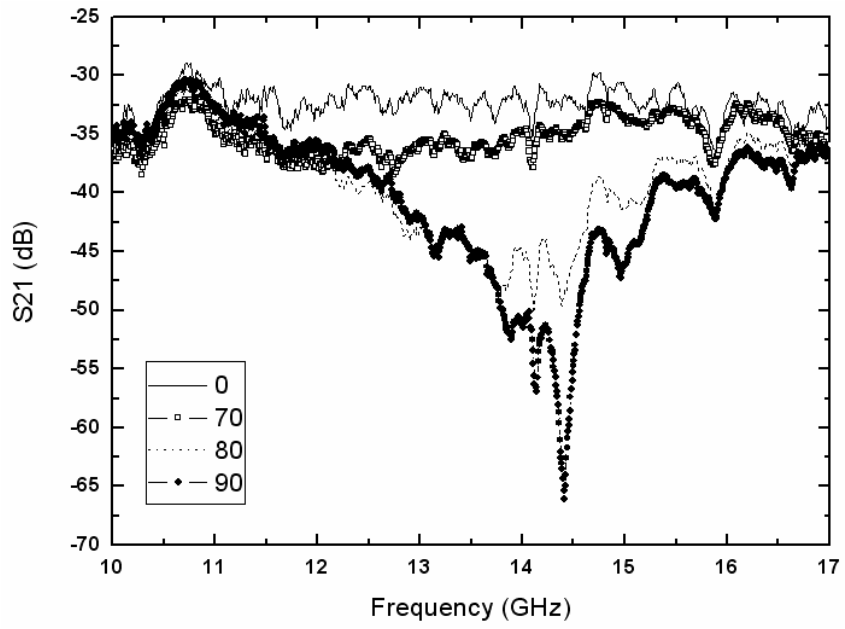

Figure 3.7: Measured transmission characteristics of symmetric DSRRs. There are four different angles in the diagram. The response of 0 degree incident is presented by solid line; the result of 70, 80, and 90 degree incident are shown by clear rectangles, dot line, and solid circles respectively.

Wire1: f = 2.135mm

Since the deepest absorption occurs at 90 degree incident, where both symmetric DSRRs and wires should exhibit their negative features, then we will focus the performance of the composite media at 90 degree. In this situation, magnetic field will penetrate the patterns, and electric field is parallel to wires.

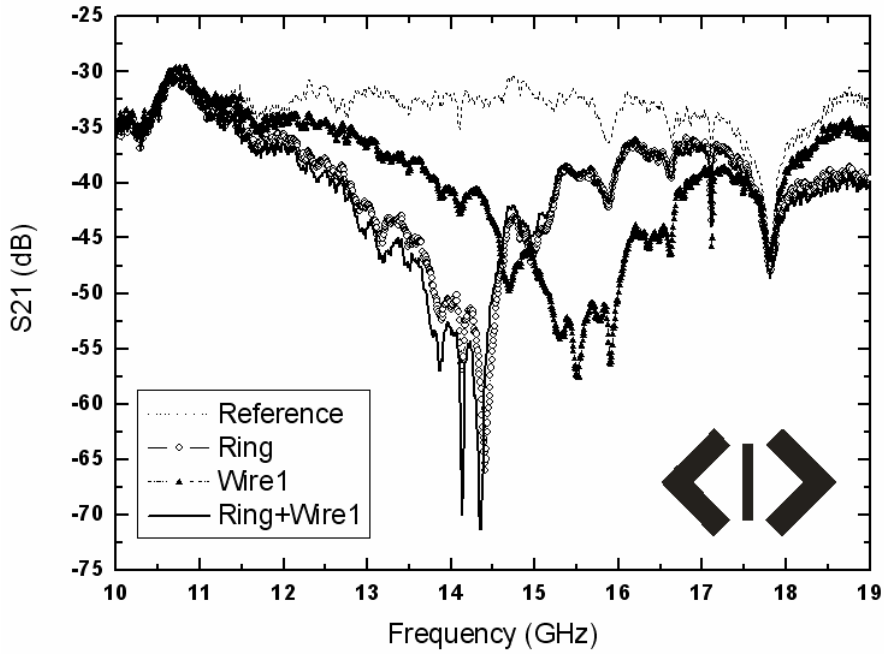

Figure 3.8: Transmission characteristics of symmetric DSRRs and wire1. The reference is presented by dash line; the result of symmetric DSRRs is shown by clear circles, and the behavior of wire1 is displayed by solid triangles. The final response of composite wires and symmetric DSRRs is denoted by bold solid line.

The measured transmission characteristics of symmetric DSRRs and wire1 are displayed in Fig. 3.8. First, the dash line presents the reference response. The data show that the response from 10GHz to 19GHz without any objects in free space has a little fluctuation. Nevertheless, the main purpose in this experiment is to observe the phenomena of negative permittivity and permeability, then the apperance of absorption is the most important concern. In consequence, the relative response between free space and patterns is the major interest even the reference power has small variation.

The result of only symmetric DSRRs has been discussed previously. As shown in Fig. 3.8, it appears a stop band around 14.41GHz. Regarding the discontinuous wire1, it also shows an absorption around 15.50GHz which just coincides the former assumption. According to the preposition, there should be some enhancement where both permittivity and permeability are simultaneously negative. In this experiment, the phenomena should occur around 14.75GHz. Notwithstanding, the measured

cooperative reaction of symmetric DSRRs and wires displayed by bold solid line does not behave as expected metamaterials. Instead of that, it shows an absorption around 14.35GHz which exhibits a similar mechanism of the symmetric DSRSs. Thus by combining these two negative mediums, the absorption does not disappear, and the enhanced phenomenon is not observed. It is almost impossible for this combination of wire1 and symmetric DSRRs to be composite metamaterials.

Wire2 and Wire3: f = 2.444mm and 2.753mm

After discovering the behavior of composite symmetric DSRRs and wire1, now the second and third types of wire – wire2 and wire3 should be explored. First of all, the responses of reference and symmetric DSRRs illustrated in Fig. 3.9 have been discussed in previous sections. The point now should focus on the behaviors of wire2, wire3 and their individual compounds. Just as Fig. 3.9 shown, there is no apparent dissimilarity between the responses of wire2 and wire3; the only observable difference is the absorption value of wire2 and wire3. If we compare these two samples carefully, the original absorption point of wire2 at 15.49GHz shrinking about 6dB when the sample is changed to wire3 is detectable. Meanwhile, the experiment results of wire2 and wire3 remind us the similarity to wire1 as well. The reason why these three kinds of wires have analogous activities may be caused by the minute length difference. The length difference, which is 0.618mm maximum, is so small comparing to the operating wavelength that external electromagnetic waves may not sense the variation at all. Hence we can not find distinct transmission characters between them.

In contrast to the observable power variation, the behaviors of wire2 compound and wire3 compound is almost identical except for an extremely subtle shifting of resonant frequency by 0.02GHz which can not be sensed from the Fig. 3.9. Such a tiny difference means that the action of wire2 compound and wire3 compound can be viewed as the same pattern eventually. Thus the relation between wire1 compound and wire2 compound can expand to that between wire1 compound and wire3 compound either. In general, the curve of wire2 and symmetric DSRRs is a little different from that of wire1 compound because the wire length has introduced a

slight interruption inside the gap of two halves of a single symmetric DSRR. In fact, the absorption becomes narrower, and the resonant frequency shifts slightly to higher frequency by 0.23GHz when the curve of wire1 composite medium totally imitates the reaction of symmetric DSRRs structure. Consequently, this composite medium with a sharp absorption does not reach the aim of implementing metamaterials. The absence of enhancement indicates that the composite wire2 and wire3 structure do not satisfy typical characteristics of metamaterials.

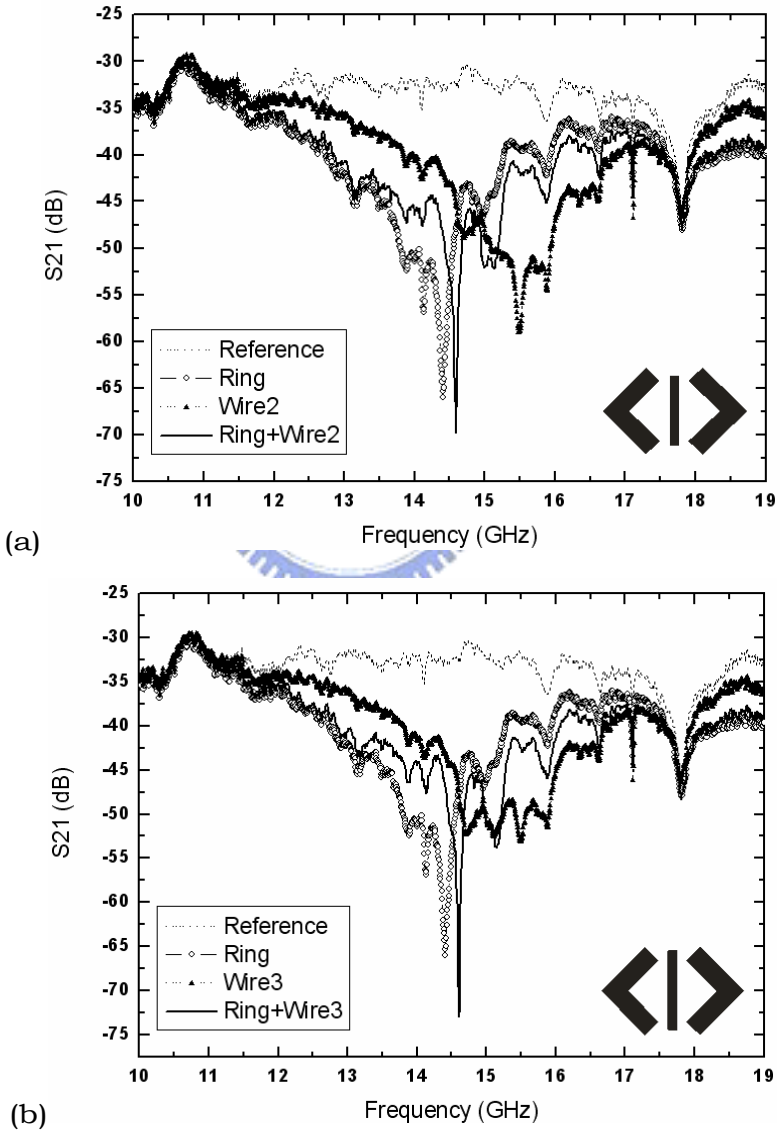

Figure 3.9: (a) S21 parameter of symmetric DSRRs and wire2. (b) Measured Transmission response of symmetric DSRRs and wire3.

In spite of the failure of implementing metamaterials, the latent difference between wire2 and wire3 together with symmetric DSRRs might be against to our prior assumption. That is, the wire length should dominate the total behavior of the combined medium. Unfortunately, the experiment data brings a totally distinguish prospect from that; a subtle modification of the wire length inside the gap does not bring significant distinction.

Wire4: f = 9.186mm

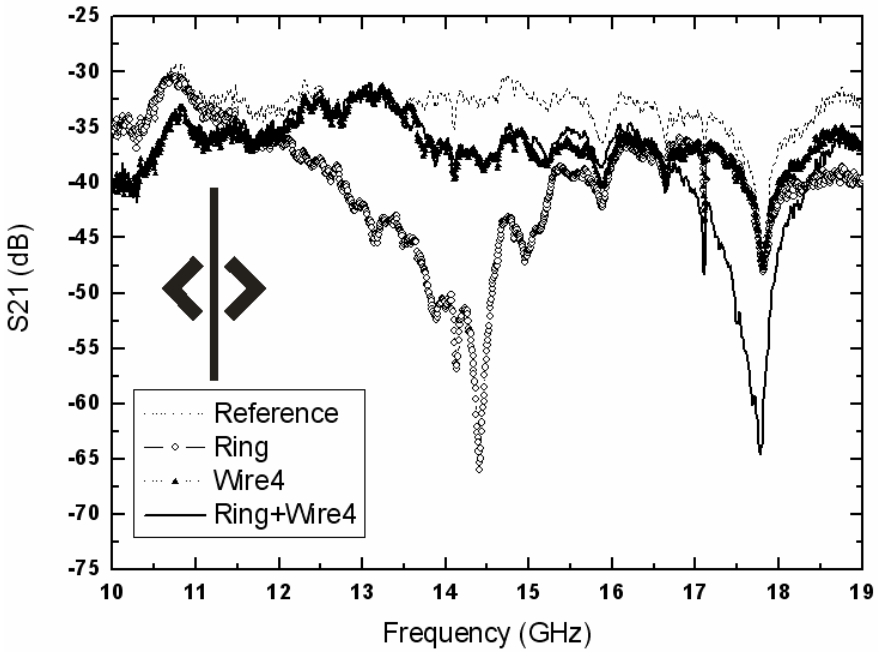

Figure 3.10: Transmission characteristics of symmetric DSRRs and wire4. The important behaviors of wire4 and its composite structure are displayed by solid triangles and bold solid line respectively.

The measured transmission characteristics of symmetric DSRRs and wire4 are depicted in Fig. 3.11. The results of reference response and only symmetric DSRRs have been discussed in earlier words. Now the response of wire4 must be emphasized. As shown in Fig. 3.11, the measured scattering parameter of wire4 is much different from wire1 to wire3. A curve approaching reference response replaces the appearance of stop band. The estimated absorption phenomenon does not appear. In fact, the response of wire4 alone acts much like the behavior of continuous wires with the

absorption less than 5 dB. As for the cooperative reaction of symmetric DSRRs and wire4 displayed by bold solid line, it does not behave as metamaterials. In contrast to that, the composite medium is almost the same with the reaction of wire4 alone despite a 20 dB drop around 17.77GHz. Thus the combination of these two patterns is dominated by the wire structure. The composite medium of wires and symmetric DSRRs does not have manifest interaction with incident electromagnetic fields because the wires possess an important role in the combined patterns.

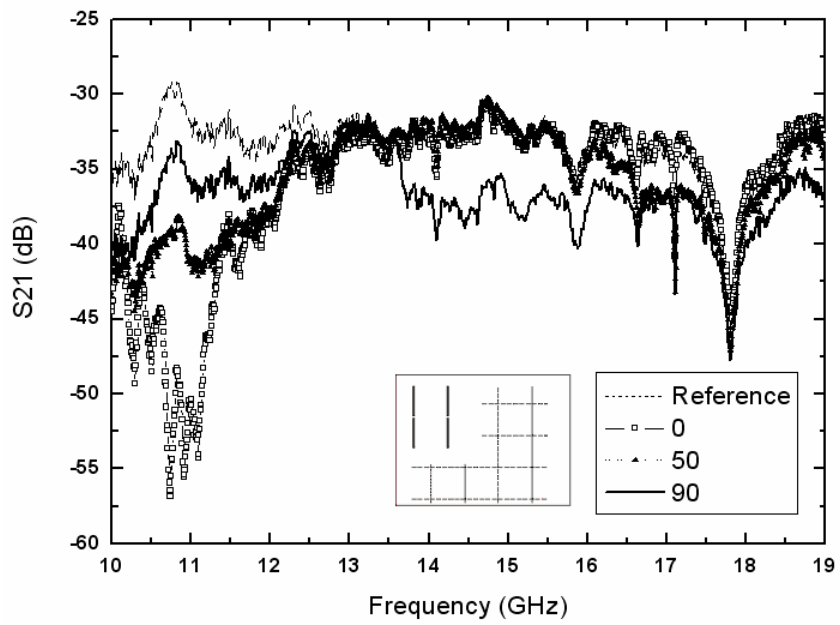

Figure 3.11: Measured transmission response of wire4. The reference is presented by dash line; the result of 0 degree incident is shown by clear rectangles. When the pattern rotates to 50 degree, its response is denoted by solid triangles while the bold solid line presents the 90 degree incident.

In order to clarify the actual property of wire4, an additional spectrum by rotating it from 0 to 90 degree is shown in Fig. 3.12. The most interesting phenomenon observed through the spectrum is the response of pattern at 0 degree incident. With this perpendicular condition between the PCB slit and incident beam, there is a drop around 11GHz. The stop band occurs at 0 degree is so strange that the phenomenon should be distinguished from the property of negative permittivity. As

the PCB slit rotates to 50 degree, the abrupt absorption disappears and becomes a smoother curve which is labeled by solid triangles. The tendency continues while the rotation angle increases from 50 degree to 90 degree. An even flatter curve denoted by bold solid line exhibits the similarity with reference; that is, wire4 structure at 90 degree may neither cause any phenomenon nor have physical reaction with incident microwave. Its behavior is totally different from any cut wire mentioned above.

3.3 Simulation Exploration / Verification

After getting the experiment results above, a further discussion of comparing practical experiment with ideal simulation is also essential. Here commercial software named High Frequency Structure Simulation (HFSS) by Ansoft is chosen for the coplanar structure at high frequency electromagnetic range.

3.3.1 Environment Setting for Simulation

Due to the restriction of hardware and time, the environment setting would be slight different from the practical experiment setup. Since the total number of coplanar metamaterials is a large amount and the measurement is operating in free space, it will be extremely difficult and unrealistic to simulate such a condition in any simulation tool. Consequently, the trade off between accuracy and time is an important issue; consuming less time and getting adequate accuracy is the first concern. In other words, the balance between time accuracy must be obtained. Therefore, the emphasis should be focused on the trend or phenomenon of coplanar structures, and the exact resonant frequency is not as important as the relative relation between various structures. In order to match this requirement, the practical free space propagation is not suitable anymore. A more efficient waveguide whose size is $20 \times 20 \times 20\, mm^3$ with 7.5GHz cutoff frequency will replace it. Moreover, the total number of the coplanar units is reduced to 4 (2 cells in one row and 2 cells in one column) to get the balance between accuracy and time consuming.

3.3.2 Simulation Results

Symmetric DSRRs

First, the simulation result of 2x2 symmetric DSRRs units is shown in Fig. 3.13 (a). The scattering parameter S21 denoted by solid line shows an obvious absorption whose minimum value locating at 20.18GHz. According to precedent discussion, the resonant frequency will drift to higher part while the total cell number of units decreases so that the simulation coincides with the actual trend exactly. Since the size of 2x2 symmetric DSRRs is much smaller than experiment sample (10x10), then it is very reasonable to get a higher resonant frequency in the simulation.

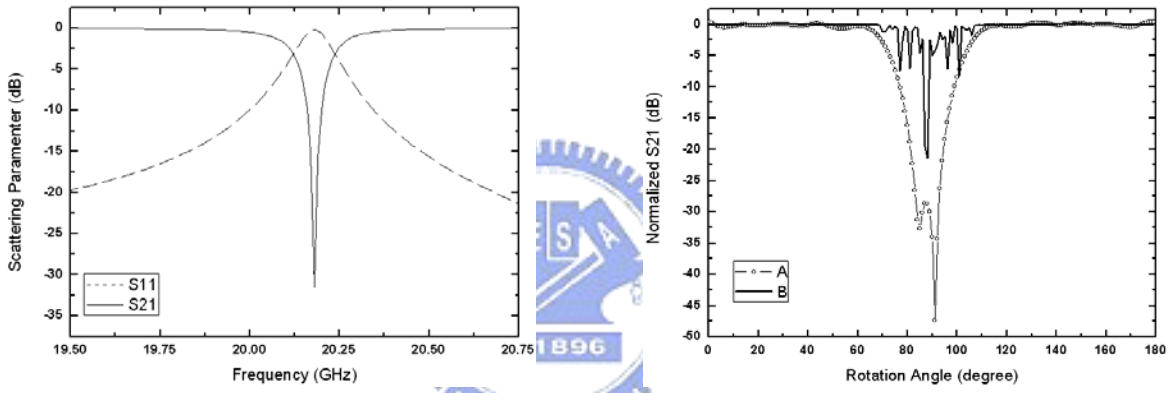

(a) (b)

Figure 3.12: (a) The simulation spectrum of symmetric DSRRs structure. A stop band appears at 20.18GHz. (b) The normalized absorption spectrum versus rotation angle. Curve A presented by clear circle indicates the measured experiment results. Curve B is the response through simulating calculation. The resolution of both curves is 1 degree.

Next, the relationship of transmitting parameter S21 and the rotation angle should be discussed by fixing the resonant frequency. The final results for comparing simulation and experimental data are illustrated in Fig. 3.13 (b), and the resolution for both curves is 1 degree as well. After normalizing the data gathered from experiment, curve A shows a smooth curve with a deepest absorption at 90 degree. A direct simulation outcome presented by curve B has similarly absorption

phenomenon at the neighborhood of 90 degree except for the maximum drop appearing at 88 degree. The slight shift may be caused by the different environments of simulation and experiment. However, the trend of absorption, which occurs from 60 to 120 degree for both simulation and experiment, indicates similar physical phenomenon.

Wire1: f = 2.135mm

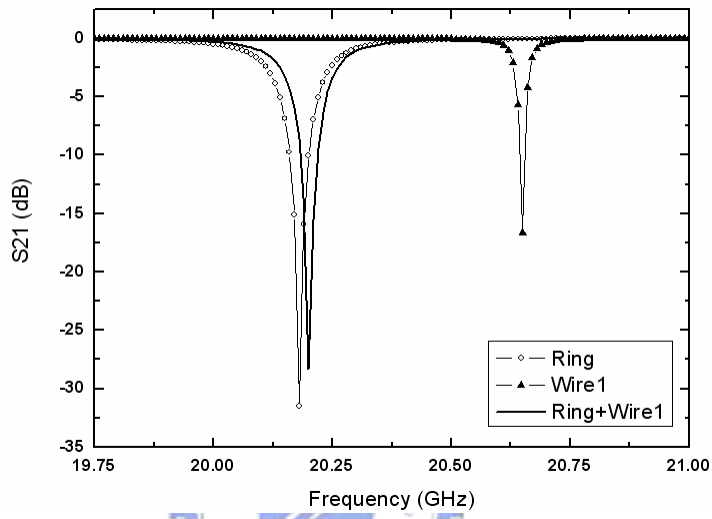

Figure 3.13: The comparison simulation results between wire1 and its compound medium.

Fig. 3.14 shows the simulation results of composite symmetric DSRRs and wire1. The absorption of symmetric DSRR (ring) structure has been discussed previously. Now, the relative response of wire1 and the composite medium is the focus of concern. First of all, there is absorption at 20.65GHz showing the response of wire1 structure to the incident microwaves. The resonant frequency of wire1 is higher than that of the symmetric DSRRs, which is identical to the experiment results. Moreover, a stop band appears at 20.20GHz displaying the total reaction of the combined wire1 and symmetric DSRRs. As mentioned before, the resonant frequency of symmetric DSRRs alone locates at 20.18GHz, hence it is lower than that of the composite medium, say, 20.20GHz. Although the relation between these two resonant frequencies is not exactly similar, the differential value of them is too small to tell. Thus the simulation results approximately coincides with experiment ones except for

the small relative position between composite medium and symmetric DSRRs alone.

Wire2 and Wire3: f = 2.444mm and 2.753mm

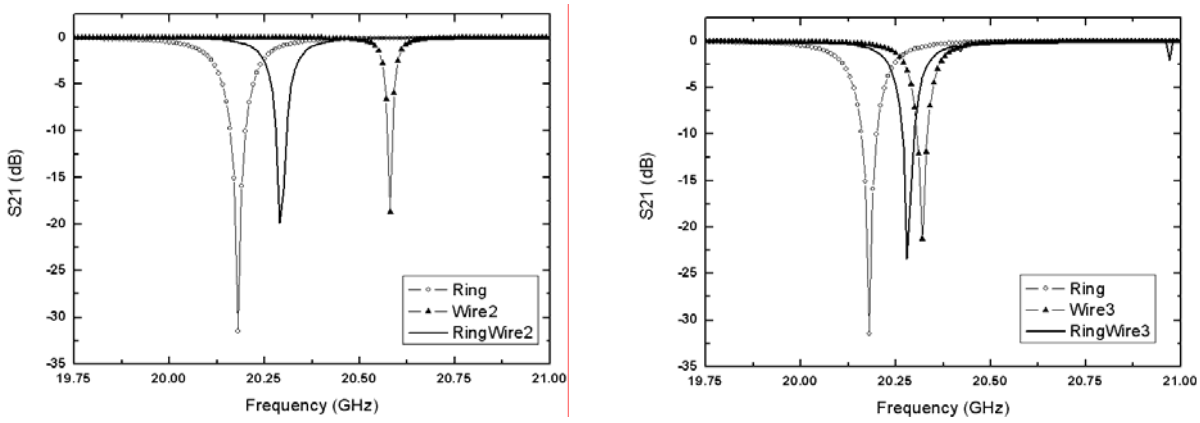

(a) (b)

Figure 3.14: (a) The comparison simulation results between wire2 and its compound medium. (b) The comparison simulation results between wire3 and its compound medium.

According to foregoing experiment data, the reactions of wire2 and wire3 are almost identical, hence the simulation results can be analyzed and discussed together in order to obtain clear vision. In Fig. 3.14 (a), the trend of response for these two samples is quite similar to that of wire1. The resonant frequencies of wire2 and wire2 with symmetric DSRRs are 20.58GHz and 20.29GHz respectively. Meanwhile, the resonant frequencies of ring, wire2, and wrie2 plus symmetric DSRRs are in the same order with that of experiment results despite all their frequencies shift. Moreover, the resonant frequency of wire2 changes from 20.65GHz (resonant frequency of wire1) to 20.58GHz while the experiment data shows barely difference. The main reason why the resonant frequency of wire2 decreases in the simulation is the scale of the space of environment. In experiment, the size of ordinary sample is about $20 \times 20\, cm^2$ and the experiment space is around $60 \times 40\, cm^2$. In contrast to the huge scale of realistic experiment environment, the range of simulation is very small, which is only $2 \times 2\, cm^2$. The volume of simulation environment is sole 1/00 of the experiment one; such a small scale will make the variation of wire length bring huge impact to the whole system while it does not affect the experiment results. Therefore, it is rational

to see the resonant frequency of simulation drifts when the wire length has slight difference. Meanwhile, the same effect can explain the behavior of wire3 as well, including the shift of resonant frequency (20.32GHz) of wire3 alone.

Wire4: f = 9.186mm

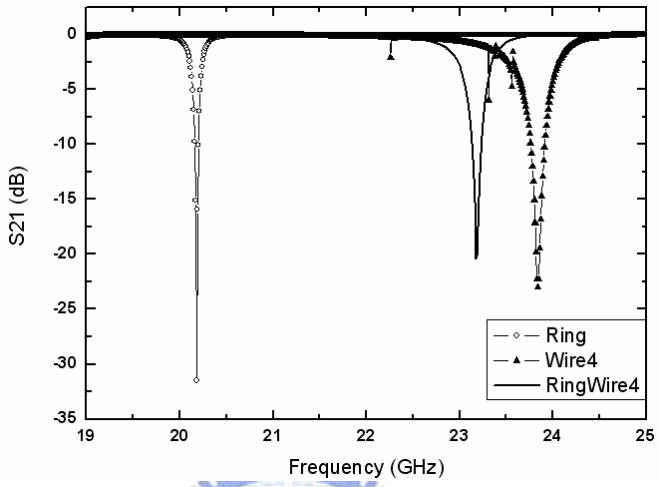

Figure 3.15: The comparison simulation results between wire4 and its compound medium.

Finally, the simulation results of wire4 and its composite medium is under survey. As shown in Fig. 3.17, the response of wire4 has a resonant frequency at 23.84GHz while its compound has a resonant frequency at 23.18GHz. Comparing the simulation response to the experiment data, the trend of wire4 plus symmetric DSRRs and symmetric DSRRs alone is the identical. Nevertheless, the behavior of wire4 is quite distinguished between simulation and experiment because the experiment results do not show the absorption curve of wire4 in the spectrum. The reason why the absorption curve does not appear in experiment may be caused by the limitation of the experiment equipments. Since the location difference of wire4 and wire4 plus symmetric DSRRs is only about 1GHz, there is huge chance for the difference in experiment has the same value around 1GHz. If the difference exceeds 1GHz, then the absorption curve will not locate in the observed region (10GHz ~ 19GHz), thus the response of wire4 alone in experiment seems to be invariant.

Next, the spectrum of wire4 alone versus the rotation angle is necessary as well.

The absorption relation of 0 degree and 90 degree shown in Fig. 3.18 is very clearly. The reaction of normal incident is much deeper than that of parallel incident. This coincides with the phenomenon in experiment. Moreover, another issue which is deserved discussion might be the resonant frequency of simulation. The central point of the absorption curve is at 11.74GHz while the experiment one locates at around 11GHz. The tiny variation between simulation and experiment results at 0 degree concluds that the absorption curve for wire4 is not caused by negative permittivity. There are two reasons which may explain why the absorption of wire4 is not due to negative permittivity more clearly.

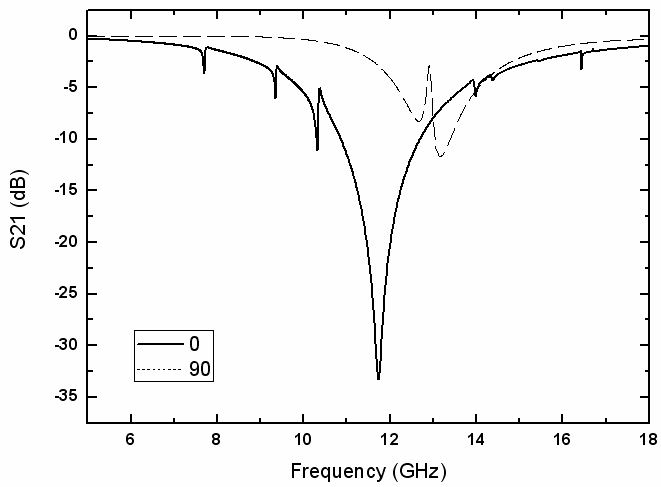

Figure 3.16: The simulation results for wire4 alone at different angles.

First of all, the resonant frequency of wire structure due to negative permittivity varies with the cell numbers. Thus, the resonant frequency of simulation and experiment should be extremely different (4 cells in simulation versus 100 cells in experiment) just like what wire1, wire2 and wire3 do. Hence, the absorption of 0 degree should occur at higher spectrum, but it does not. This is one of two reasons that the absorption is not caused by negative permittivity. Another factor that negates the existence of negative permittivity is the rotation angle where absorption occurs. Since the property of negative permittivity of cut wires can only be realized while the incident microwave is parallel to the sample, the physical reaction for wire4 at normal incident is definitely some other physical response distinct from that. In

conclusion, the wire4 structure is out of the exception of negative permittivity. Instead of that, it might be the phenomenon of grating effects which is not affected by cell numbers and appears at normal incident.

3.4 Discussion and Conclusions

After examining all experiment and simulation results, the physical meanings of symmetric DSRRs and discontinuous wires need to explain. Our discussion will be emphasized on three aspects; they are the physical activity of symmetric DSRRs, response of wire structures, and the corresponding behavior between wires and symmetric DSRRs.

The symmetric DSRRs not only present the property of negative permeability but also display the main factor determining the resonant frequency. As mentioned previously, the experiment and simulation data of symmetric DSRRs exhibit the exact existence of negative permeability. The resonant happens as the propagating direction is parallel to the PCB, where magnetic field penetrates symmetric DSRRs. At this moment, the external magnetic field passing the ring structure generates strong currents flowing along two half rings of a symmetric DSRR. Charges excited by this surface current would accumulate at the opposite proximity of each half part. The positive and negative charges which occupy against the small gap hence introduce a strong electric field. The scheme of symmetric DSRRs is quite similar with that of DSRRs; thus it is not surprise to see symmetric DSRRs having the resonant mechanism. Furthermore, the resonant frequency of symmetric DSRRs which locates at 14.41GHz is another interesting issue to discover. The experiment results of symmetric DSRRs introduce extra accounts, the total cell unit number, involving the determination of resonant frequency. Resonant frequency should be dominated by lattice constant due to anterior knowledge. Nevertheless, the experiment data show that the resonant frequency of symmetric DSRRs with 10mm lattice constant is higher than the that of DSRRs with 5mm lattice constant. Former sample has a resonant frequency at 14.41GHz while latter possesses around 12GHz [10]. The experiment results can barely find a reasonable explanation if the results are only investigated by viewing the lattice constant. Consequently, another concern such

as the total number of units on a single sample should be included as the effective factors. Comparing to the sample of DSRRs [10] whose total number of units is 560, the total number of symmetric DSRRs in this thesis is sole 100. As we know, the resonant frequency has mighty relation with the unit number. A sample with identical lattice constant would have a lower resonant frequency when it holds more unit numbers. Therefore, with only one forth of the total unit number, symmetric DSRRs display higher resonant frequency even having twice the lattice constant. In summary, the experiment results of symmetric DSRRs are not surprised since the phenomenon of negative permeability is observed on the fundamental of the relationship between resonant frequency, lattice constant, and cell number.

Next, we want to explore the behavior of wire structures. As the experiment and simulation data shown, the response of wire1 to wire3 is barely distinct, which makes the physical explanation of them being similar. Generally, the cut wires of wire1 to wire3 only have reaction to the external incident electric field at 90 degree. In other words, the effect of negative permittivity only appears when the microwave encounters periodic wires along the propagating direction. Also, the absorption area of discontinuous wires does not extend to zero frequency on account of the intrinsic traits. In contrast to the behavior of wire1 to wire3, long cut wire, wire4, carries much disparate activity which is not actually representative negative permittivity structure. The experiment data indicates that it has stronger absorption at 0 degree rather than that at 90 degree, which means wire4 possesses different characters other than negative permittivity. The phenomenon that absorption intensity decreases as the rotation angle increases from 0 to 90 degree reminds us the physic reaction of grating. When the plate of PCB is perpendicular to the propagating direction, each metallic strip of wire4 on PCB just mimics the line grating in ordinary optical experiment. Hence the chance of constructing metamaterials will tends to zero even we put wire4 and symmetric DSRRs together. For accomplishing the goal of building negative permittivity structure, wire1, wire2, and wire3 have demonstrated the existence of it except for wire4.

After discussing ring and wires respectively, the reaction for the medium comprises these two structures needs to be discovered. The response of composite

symmetric DSRRs and wires approach the behavior of symmetric DSRRs alone according to Fig. 3.8, 3.9, and 3.10, which means their interaction with the peripheral electromagnetic waves is primarily dominated by the characteristics of symmetric DSRRs. On the contrary, wire4 is the major trait that controls the spectrum of composite wire4 and symmetric DSRRs. In Fig. 3.11, the bold line curve indicates the original response of symmetric DSRRs is totally destroyed by an introduced interruption, say, wire4, within the ring gap. The apparent absorption band which extends from 12GHz to 16GHz caused by symmetric DSRRs is eliminated, and suggests that the ring structure of composite wire4 medium does not have function as expected; external electromagnetic waves may ignore such a structure as propagating. In fact, the intuitive physical sense tells the domination of long cut wires in long wire compound and rings in short wire compound. Wire length between 2.135mm and 3.062mm should have a crucial point which may possess the property of negative permeability and negative permittivity simultaneously in our prior concept. However, the experiment data is against such a deduction. Fig. 3.9 and Fig. 3.10 point out the composite medium still holds the absorption curve even when short wires are inserted. The truth is that the composite medium will always has the absorption activity no matter how long the wire is, and the absorption is caused by either wire or symmetric DSRRs. While the wire is short enough, the behavior is controlled by symmetric DSRRs. Once the wire exceeds the length, wire structure will be takeover the response immediately. Therefore, the scheme of symmetric DSRRs and discontinuous wires is not a successful mechanism realizing metamaterials eventually.

Chapter 4

Double Resonant Frequency (DRF) DSRR

Since the concept of metamaterials had been proposed in 90s, it has inspired a lot of attention and myriad ideas of application. The ultimate target of developing metamaterials is to apply such a novel structure at the range of visible light so that people can break conventional use on optical systems nowadays. That is why many works accomplished focuses on reducing the size of metamaterials. However, even the difficulties of manufacturing issue for metamaterials at light region are concurred, there is still a serious problem involving terrible power efficiency for realistic applications. In this chapter, the idea of fractal-like will be utilized to compensate the power loss. First, the original concept of fractal and the inheriting fractal-like idea for double resonant frequency (DRF) DSRR will be introduced. Then two types of fractal-like structure are proposed as possible solutions for this problem. Finally, physical explanations and discussions will be presented.

4.1 Inspiration of Fractal-like

4.1.1 Concept of Fractal

“Clouds are not spheres, mountains are not cones, coastlines are not circles, and bark is not smooth, nor does lightning travel in straight line,” the first few sentences described in the book written by Mandelbrot in 1977 was the most central concept of fractal [13]. Before the

concept of fractal had been proposed, the world had been dominated by Euclid's "Elements" which clearly defined the integer dimension of all objects on earth. Sets and functions that are not regular or smooth enough will be ignored and not worthy for study. The attitude, however, started to change step by step about 100 years ago. Some mathematicians proposed a few "monsters" figures showing untraditional geometric configurations. They also defined new dimension which is not being integer for these monsters. The study for such untraditional geometric frames continued in the following decades. In 1977, due to the development of computer, Mandelbrot summarized all ideas and named "*fractal*" to this field of study. He claimed that many patterns of nature are so irregular and fragmented that nature exhibits not simply higher degree but altogether different level of complexity. Therefore, he conceived and developed a new geometry of nature which can describe many practical cases in the world. Also, the most important role in this work is the *fractal dimension* (Hausdorff dimension) that describes configurations in a way different from Euclid's concept.

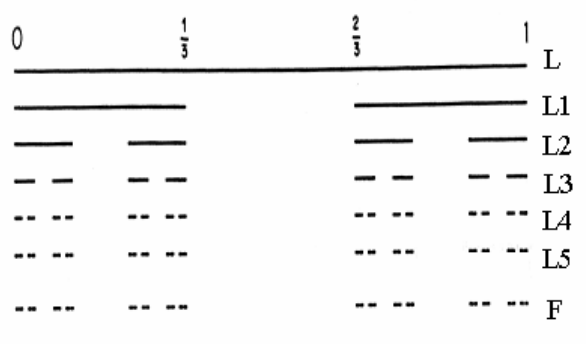

Figure 4.1: Construction of the middle third Cantor set F, by repeated removal the third of intervals [14].

The middle third Cantor set is one of the best known and most easily constructed fractal; nevertheless it displays many typical fractal characteristics. The construction of it will begin from a unit interval by a sequence of deletion operations as shown in Fig. 4.1. The first step is to delete middle third of L so that only interval [0,1/3] and [2/3,1] survive. Similar recursive steps will continue from L1 to L2 and so on. Here,

L_k consists of 2^k intervals each of length 3^{-k} and F may be thought of as the limit of the sequence of set L_k as k tends to infinite. It is obviously impossible to draw such an infinitesimal set of F hence picture of F tends to be one of the L_k, which is a good approximate of F when k is reasonably large. In fact, the set of F will be seen as infinite points (which are considered as zero dimension in traditional geometry) instead of segments of a single line (which are considered as one dimension in traditional geometry) while k tends to infinite. The intuitive instinct is slight different from geometric definition thus the fractal dimension, which is first proposed by Hausdorff, is necessary. The definition of fractal dimension is :

$$D = \frac{\ln(N_\delta)}{\ln(1/\delta)} \tag{4.1}$$

where N_δ is the number of segment after each iterative step and δ is the ratio of the length after each operation to that before each operation. From Fig. 4.1, the fractal dimension of middle third Cantor set will be

$$D = \frac{\ln(N_\delta)}{\ln(1/\delta)} = \frac{\ln(2)}{\ln(3)} = 0.631 \tag{4.2}$$

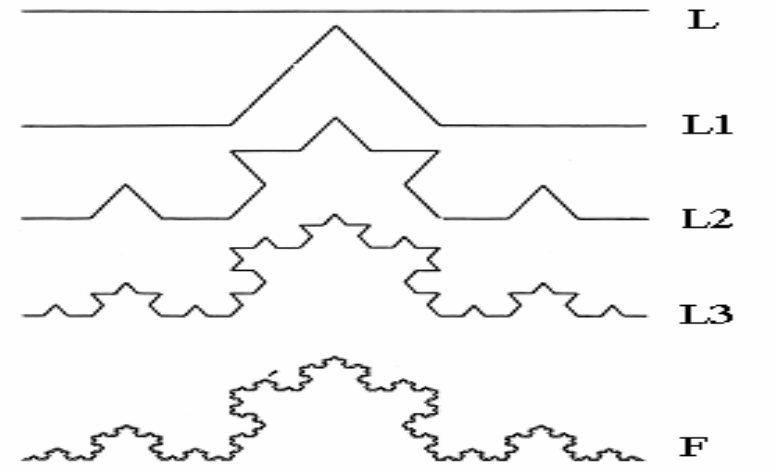

Figure 4.2: Construction of the von Koch curve, by repeated removal the middle third of each ling segment and replacing it by another two segments equal to remain parts [14].

The fractal dimension of the middle third Cantor is neither one dimension (1-D) nor zero dimension (0-D). It is a kind of configuration locating between 0-D and 1-D. A

further example of famous von Koch curve shown in Fig. 4.2 can give an even clearer vision of fractal dimension. The initial length of Koch curve is set to be unit length. L1 consists of four segments obtained by removing the middle third of L and replacing it by the other two sides of the equilateral triangle based on the removed segment. In other words, the parameters N_δ and δ are 4 and 1/3 respectively thus the fractal dimension will be 1.262 which is neither 1-D nor 2-D structure. In fact, as k tends to infinite in developing von Koch curve, the set F will approach filling the whole surface of the trace which seems to be 2-D frame while it will be still considered as 1-D frame in traditional geometry.

In conclusion, the concept of fractal could be used to describe most of the patterns which are originally thought to be irregular or amorphous existing in our mother nature. Since Mandelbrot proposed this concept in 1977, it has been widely applied to various areas including biology, geology, astronomy, and chemistry. People in diverse fields try to find out a rule explaining for most frames through fractal. With no exception, there are also numerous studies of fractal for electromagnetism. The best known application of fractal for microwave is the fractal antenna which can promote the bandwidth and radiation pattern due to its high characteristic of self-similar. Therefore, basing on the successful experience of fractal antenna, we wonder if it is possible to apply fractal or fractal-like techniques on metamaterials. Could it help to countervail the insufficient power transmission of intrinsic metamaterials just like it does for the fractal antenna? In the next subsection, the combination of fractal-like skill and metamaterials will be introduced in order to discover the possibility of compensating the power loss of metamaterials.

4.1.2 Implement of Fractal-like Concept on Metamaterials

Power insufficiency is always a problem of metamaterials when it is utilized within the range of visible or infrared range. Fortunately, the successful experience of fractal antenna brings some hints for conquering the unsolved issue. Basing on the extension of the percept of fractal, a DSRR structure contains two different lattice constants mimicking fractal is proposed and shown in Fig. 4.3.

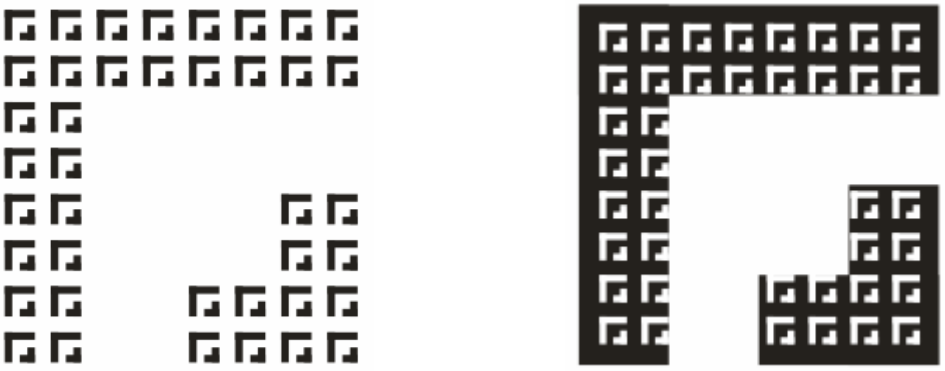

(a) (b)

Figure 4.3: Two different implementations of double resonant frequency DSRR. (a) One of the methods to construct the structure with two lattice constants at the same time. (b) Another way to build up double resonant frequency DSRR.

These two patterns are not actually fractal because they do not obey its strict definitions; they are just similar to the concept of fractal, so that is why they are called fractal-like. Since this structure has large and small DSRRs simultaneously, there should be double resonant frequency while doing the experiment. In the design, there are two methods to realize the idea of double resonant frequency. The first one is to fill up the larger DSRR by smaller ones, and another one is to excavate smaller DSRRs from a complete larger DSRR. We hope that there would be some interaction between two kinds of DSRRs in different scales while their corresponding resonant frequency is observed respectively. Moreover, if there is indeed some interaction, the absorption power of them could be utilized to retrieve the insufficient power of the other one. In the next two sections, details of implementing these two double resonant frequency samples will be introduced and described clearly. Some experiment results and discussions will also be included as the demonstration.

4.2 DRF-DSRR Basing on Split DSRR

Divide the larger DSRR into numerous small DSRRs is the first method to realize the double resonant frequency structure, thus this structure is named Split DSRR

(SDSRR). While the small DSRRs is small enough, the lager one will be considered as a complete unit of negative permeability medium. This novel property may provide the solution for the unsolved power issue. In this section, the implementation of DRF-DSRR basing on SDSRR will start from a pre-experiment with a small gap on the ordinary DSRRs.

4.2.1 Pre-experiment: Design and Experiment of SDSRR

Before start the experiment of double resonant frequency basing on SDSRR, a pre-experiment needs to be done first in order to obtain preliminary evidence to demonstrate feasibility of SDSRR. Moreover, the experiment results can provide useful information for further estimation as well.

Design

The idea of pre-experiment is to dig several gaps in the middle of DSRR just like Fig. 4.4 shown. The schematic drawing of SDSRR is similar to DSRR except for four straight gaps whose width is 0.2mm. Despite the gap, other restrictions such as linewidth *d* and lattice constant are all the same with that of original DSRRs.

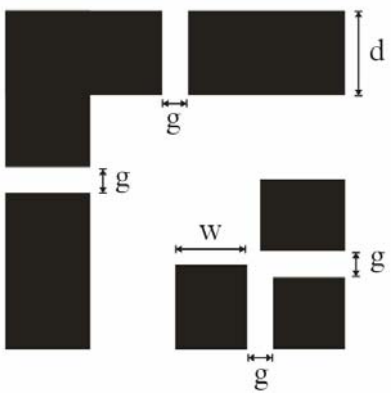

Figure 4.4: Schematic figure of a single split DSRR (SDSRR) shows four straight gaps *g* whose width is 0.2mm. Linewidth *d* is 0.655mm and *w* is equal to 0.555mm.

Imitating a completely original DSRR by so many small DSRRs is the initial

inspiration of accomplishing DRF pattern. In such a structure, gaps between different small DSRRs are the most crucial factor of success. Therefore, the design of SDSRR which holds four gaps is set to be the pre-experiment, and helps to supply proper knowledge. If the absorption will appear even with gaps within DSRRs, then there is great chance for SDSRR to build up the DRF pattern. On the contrary, if the reaction between SDSRR and external microwaves does not present apparent absorption, the possibility of implementing SDSRR into DRF pattern will be quite minute.

Sample Specification and Experiment Environment

In experiment, SDSRRs alone will be measured. The cooperative response of them with continuous wires whose radius is 0.15mm and plasma frequency is 18.20GHz basing on Sarychev and Salaev's deduction [15] will be detected as well. The lattice constant of SDSRRs is still 5mm which is only half of that in Ch.3. Here SDSRR patterns are made by copper. All metallic media that consist of periodical arrangement of wires and SDSRRs are fabricated on PCB, whose specification is the same as that in Ch.3. However, in this experiment, metallic wires and SDSRRs are manufactured in opposite faces of a single PCB, thus wires and SDSRRs will not disturb each other. The total number of units on per PCB is 500 (25 cells in one row and 20 cells in one column). Moreover, the experiment environment is exactly the identical to that in Sec.3.2.1.

Experiment

The spectrums of SDSRRs and SDSRRs with wires at 90 degree incident are displayed in Fig. 4.5. Absorption curve of SDSRRs themselves only appear while the rotation angle approaches 90 degree; absorption phenomenon does not occurs as the incident microwave is perpendicular to the patterns. Thus, the discussion can focus on the behavior of SDSRRs at parallel incident condition. First, free space reference marked by dot line presents the intrinsic spectrum of network analyzer itself. The variation of free space response is acceptable since the relative response between free space and SDSRRs is more important than the absolute values of absorption. Next, we are going to discuss the behavior of SDSRRs themselves. The maximum drop of

SDSRRs happens at 14.94GHz, and it has a difference of 29.49dB corresponding to free space reference. This power drop presents the existence of negative permeability even when there are four gaps across the linewidth of each original DSRR. When the periodic wires are adding to the opposite plane against SDSRRs on a single PCB, the cooperative behavior is presented in Fig. 4.5 as well. A manifest enhancement that approaches 26dB around 15GHz is observed, which means successful experiment results as expected. In other words, real propagation constant with negative value is obtained when metallic thin wires possessing negative permittivity and SDSRRs holding negative permeability both exhibit simultaneously around 15GHz.

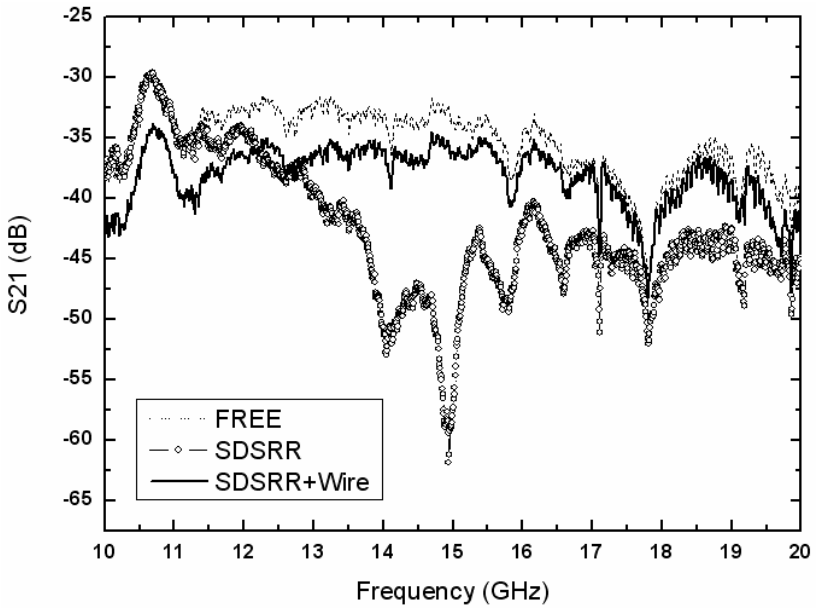

Figure 4.5: Transmission properties of SDSRRs and their response adding wire structure at parallel incident. The free space reference is presented by dot line; the result of SDSRRs themselves is shown by clear circles, and the response of composite wires and SDSRRs is denoted by bold solid line.

The success of SDSRRs is extremely important because it maintains the fundamental properties of negative permeability even being modified by excavating several gaps. This evidence could provide truly preliminary information and support that there would be great chance for SDSRRs to accomplish DRF pattern, thus it is worthy doing forward design and experiment in the next few subsections.

4.2.2 Design for DRF-DSRR Basing on SDSRR

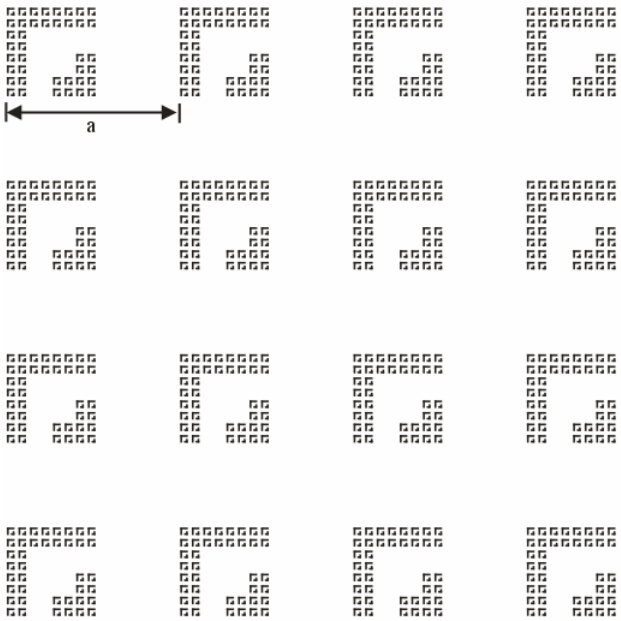

Figure 4.6: Schematic layout for DRF-DSRR basing on SDSRR. Each lager DSRR consists of 40 small DSRRs. The lattice constant a is set to be 60mm while the lattice constant of small ones is 4mm. The linewidth of small DSRRs is still 0.655mm.

The overall design of DRF-DSRR basing on SDSRR is presented in Fig. 4.6 as the details of a single unit have been shown in Fig. 4.3 (a). It has been fully considered through the limitation of experiment equipments and fabrication techniques. Due to the restriction of network analyzer, frequency exceeding 20GHz is not acceptable. Hence it is impossible to manufacture small DSRRs with lattice constant less than 4mm. On the other hand, the resonant frequency of large DSRRs should not be smaller than 1GHz because it will be extremely inconvenient to build up the setup and to measure. Therefore, two frequency regions around 1GHz and 15GHz, which make a compromise of facilities limitation, are chosen as the investigated spectrums. Their corresponding ratio, 15GHz to 1GHz, is 15.

As shown in Fig. 4.6, each large DSRR is composed by 40 small ones whose lattice constant is 4mm. Meanwhile, the lattice constant a of large DSRR is 60mm which is just 15 times of that of small ones. Since the value of lattice constant times resonant frequency should be constant, then it is very reasonable that the lattice constant of large DSRRs is 60mm by setting 1GHz as the desired resonant frequency

In the following experiment verification, two different frequency ranges will be measured around 1GHz and 15GHz. The higher and lower parts of spectrum are for smaller and larger DSRRs respectively. With 4x4 units of large DSRRs, as shown in Fig. 4.6, the higher spectrum will be observed first. Another sample contains 16x12 units of large DSRRs is measured around 1GHz in the end. The experiment setup has already been shown in Fig. 3.6 except that the horn antennas are replaced by two standard gain horns whose operating frequency are about 1GHz (Rozendal Asociates, RA3150-1; operating frequency range is from 800MHz to 1200 MHz). Furthermore, the distance between antennas and the center of sample changes from 30cm to 300cm. After separate measurement, a special measurement combines two distinct frequency area will be discovered if there are indeed some physical responses for large DSRRs.

4.2.3 Experiment Verification

High Frequency Response

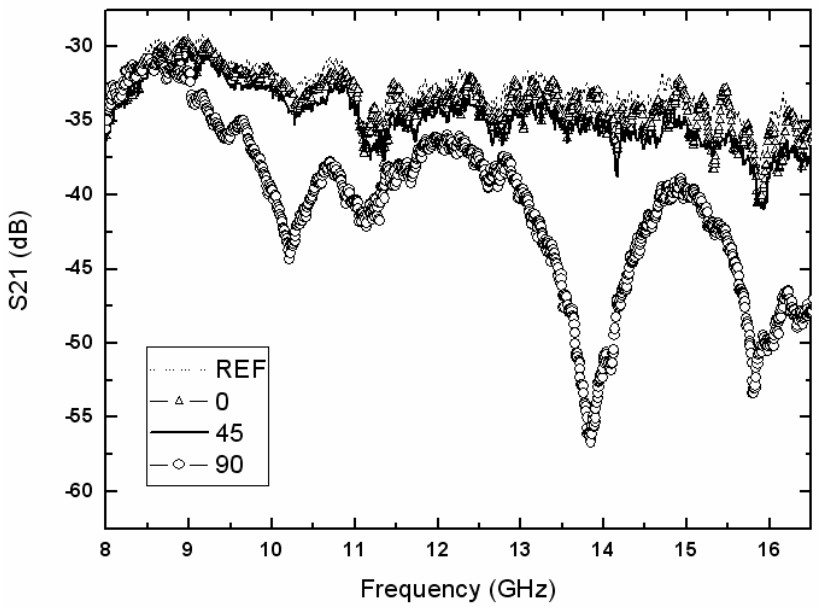

Figure 4.7: Transmission spectrum of DRF-DSRR basing on SDSRR. There are three different angles in the diagram. The response of 0 degree incident is presented by clear triangles; the result of 45 and 90 degree incident are shown by bold solid line and clear circles respectively.

Again, free space activity is presented in Fig. 4.7 as the reference, and the responses of DRF-DSRR basing on SDSRRs are under investigated as well. Obvious absorption occurs around 10GHz and 14GHz at incident angle of 90 degree. In contrast to the case of original DSRRs where only one resonant frequency is observed, the DRF-DSRR basing on SDRRs pattern at 90 degree indicates double resonant frequency. The transmission drops extending from 9GHz to 11GHz and 13GHz to 15GHz hold the value over than 10dB, comparing with the reference power. Peak absorption value appears at 13.85GHz, and the difference between it and reference power exceeds 20dB. As Fig. 4.7 shown, the physical reactions of 0 and 45 degree incident almost overlap with the reference power, which implies that external microwaves do not sense the existence of DRF-DSRR pattern at all under such as a incident condition. It also provides an indirect evidence for proving that the power drop is indeed caused by negative permeability.

Another illustration of DRF-DSRR basing on SDSRR is depicted in Fig. 4.8. It notes that the absorption is very sensitive to misalignment; a slight change of rotation angle will affect the position of resonant frequency and the strength of absorption. The characteristic of angle sensitivity only allows absorption exhibiting from 80 to 100 degree incident. Meanwhile, this trait is similar to that of other ring structures such as SRRs and DSRRs except for the double resonant frequency regions.

In fact, the property of double resonant frequency region for this DRF-DSRR pattern is due to the fractal-like scheme. In Fig. 4.6, the fractal-like design produces a lot of removal space hence the small DSRRs do not compose a complete square layout anymore. The discontinuous small DSRRs model generates the potential for incident magnetic field sensing lattice constant other than 5mm, thus dual absorptions can be detected in observed spectrum. The reason why double resonant frequency displays can be described specifically from the prospect of large DSRRs. For the linewidth of every large DSRR in Fig. 4.6, there are two rows of small DSRRs simultaneously. If each large DSRR is divided into a 4x4 areas geometrically, then it can be viewed as a complete DSRR whose linewidth is 6.62mm. Hence it is very rational for a second resonant frequency appearing.

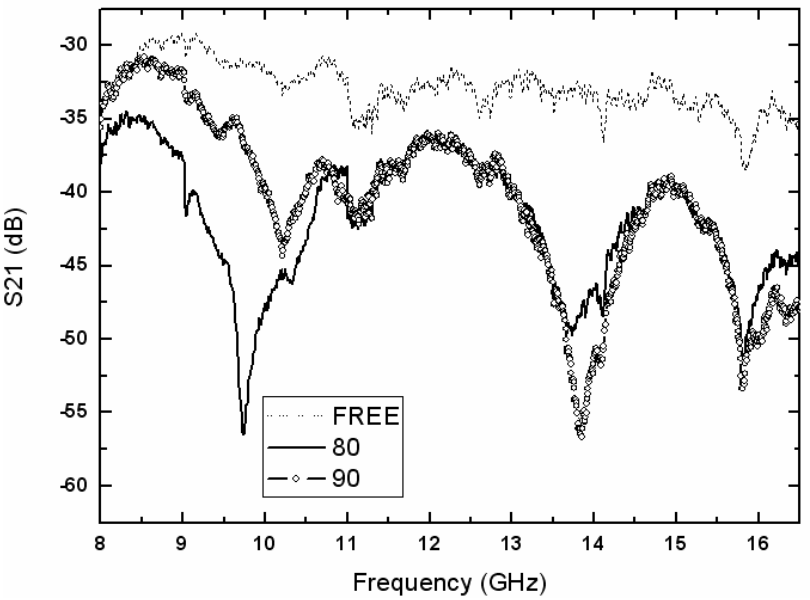

Figure 4.8: Transmission spectrum of DRF-DSRR basing on SDSRR showing the sensitivity of rotation angle. The response of 80 and 90 degree are illustrated as bold solid line and clear circles respectively.

In summary, the final results of experiment data in the range of X-band have successfully introduced the possibility for accomplishing DRF-DSRR pattern through fractal-like SDSRRs. One of the double resonant frequencies has been observed and its physical explanation has been explored. Next step, the low frequency response of large DSRR awaits further investigations.

Low Frequency Response

In the experiment for low frequency response, the pattern comprises of 16x12 large DSRR cells is placed parallel to the propagating direction of the incident microwaves, where the magnetic field penetrates all metallic structures. The measured transmission scattering parameter S21 for this sample at lower band is depicted in Fig. 4.9. Again, the activity of free space without any sample in the middle of two horn antennas is denoted by solid squares while the response of DRF-DSRR is labeled by clear triangles. Apparently, the curves of free reference and that of DRF-DSRR pattern do not have significant dissimilarity. The maximum difference is extremely small if the absorption about several decades at higher band is taken as the standard.

The difference, merely 0.82dB, might be taken as inevitable noise fluctuation of whole system instead of any meaningful physical reaction.

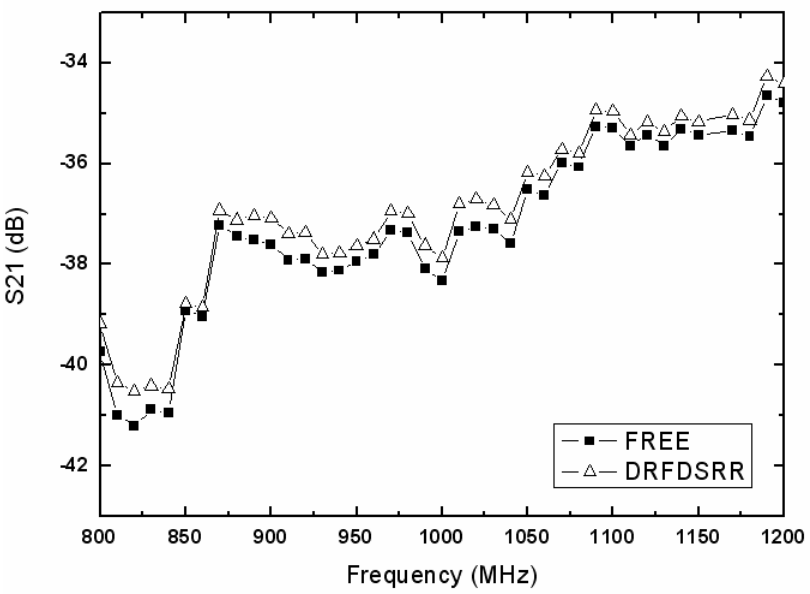

Figure 4.9: Transmission characteristics of DRF-DSRR pattern around 1GHz when the propagating direction is parallel to the PCB. Solid squares denotes the response of free space, and clear triangles indicates the reactivity of a 16x12 large DRF-DSRR array whose lattice constant set to be 60mm.

4.2.4 Summary

In summary, the behavior of DRF-DSRR basing on fractal-like SDSRR only achieves half of the estimated approaches eventually. In contrast to the positive experiment results at higher frequency, the data obtained at lower band do not coincide with the estimated supposition at all. A significant power drop around 1GHz should appear according to earlier assumption. The flat curve, however, showing the reactivity of DRF pattern to transmission power less than 0.82dB, totally annihilates original deduction, but the failure of this experiment does not mean the idea of fractal-like SDSRRs not being practical.

In fact, there are two effective reasons why the absorption phenomenon does not appear around 1GHz. The first one is that the resonant frequency may be outside the

observed region from 800 MHz to 1200MHz. the cell number of only 192 units for the pattern may introduce frequency shift in the experiment. In contrast to the range of high frequency spectrum which is about 10GHz, the lower one with 0.4GHz bandwidth is solely 4% comparing to the higher one. Therefore, any frequency change can easily shift resonant frequnecy outside the evaluated area. That might be why we can not detect any absorption through the measurement process. The second reason, which is the most important factor as well, is the poor density of each large DSRR. As shown in Fig. 4.6, there are only 40 small DSRRs in each large one. The small units can be easily distinguished from each other while viewing the whole pattern, which indicates the gaps between small DSRRs are too large. Therefore, the issue about the gaps discussed previously needs to be reconsidered. According the prior knowledge, the gaps existing between small DSRRs could prohibit the generation of flowing current within the metallic structures if they are large enough. In this case, the gaps shown in Fig. 4.6 seem to exceed the upper limitation of the width that may destroy the generation of current; hence the introduced current can not successfully be driven by the external perpendicular magnetic field. In order to eliminate such a negative factor of oversize gaps, a sample of DRF-DSRR basing on SDSRRs is going to be fabricated through semiconductor process. The scale of large DSRRs will be 5mm lattice constant while the small ones only hold the linewidth of 80nm and lattice constant of 400nm. More experiment data can provide further information and testify our prior postulation.

4.3 DRF-DSRR Basing on Inverse DSRR

The second method to realize the double resonant structure is digging small DSRRs from a metallic large DSRR. Because the excavated DSRRs are constructed by FR4, the material of PCB, they have a reverse frame corresponding to large DSRRs; hence it is named inverse DSRR (IDSRR). The method of just excavating numerous small DSRRs can eliminate the gap disadvantages of inhibiting the existence of flowing currents on metallic DSRRs. Physical phenomenon other than simply DSRRs reaction is expected to display, and retrieves the power loss. Again, the process of implementing IDSRR will begin from pre-experiment to obtain useful information

preliminarily.

4.3.1 Pre-experiment : Design and Experiment of IDSRR

Before begins the experiment of double resonant frequency basing on IDSRR, a sample other than Fig. 4.3 (b) needs to be measured to clarify the feasibility of IDSRR. Meanwhile, the experiment results can also deliver useful information for further design.

Design and Specification

The pre-experiment of IDSRR is simply constructing reverse DSRRs in square array as Fig. 4.10 shown. Black area is made by copper, and white region presents the removal of metal. Detail specifications of excavated DSRRs are identical to those in reference [10] where the linewidth is 0.655mm. Meanwhile, the lattice constant 5mm for small DSRRs will be measured in the experiment, and the total cell number is 625 (25 cells in one row and 25 cells in one column), thus it can be compared with normal DSRRs. Furthermore, the experiment setup does not change at all since Ch.3.

Figure 4.10: A part of schematic layout of inverse DSRR (IDSRR) sample for pre-experiment. Black part presents the area consist of copper and white DSRRs are the region as the metal is removed. Also, total unit number of practical experiment sample is 625 while this scheme only shows 25 cells.

Experiment

Through the experiment process, a PCB with a layer of copper on one of its two surfaces is used instead of the free space response as the reference sample to exclude any effect caused by metal itself. By rotating this reference sample, physically cooperative reactions such as diffraction and reflection between copper and the electromagnetic waves can be observed. Responses at different angles are used for the reference because phenomena of IDSRRs need their corresponding references. In Fig. 4.11 (a), a conventional spectrum at 90 degree incident is depicted. The difference between the reference sample and IDSRR pattern is hardly distinguished. They almost overlap each other in the observed zone; the behavior is far from the reaction of negative permeability. In contrast to the 90 degree incident, the spectrum where the sample is 50 degree with respect to the incident wave is illustrated in Fig. 4.11 (b). One apparent absorption band in the range from 14GHz to 17GHz displays the practical reaction of IDSRRs. The maximum value of absorption appears at 16.05GHz with over 44dB drop, which implies a phenomenon other than negative permeability as expected.

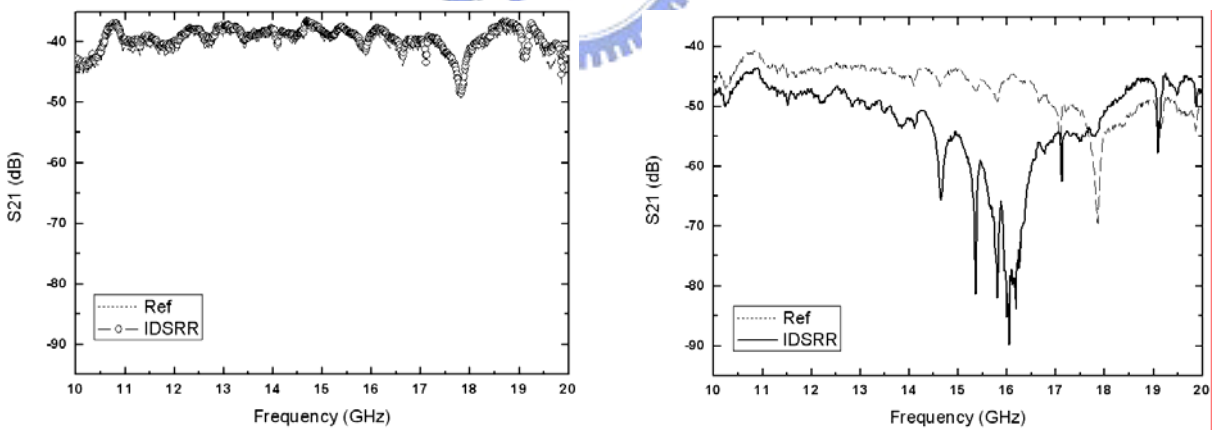

(a) (b)

Figure 4.11: (a) The spectrum of IDSRRs and its reference at 90 degree. The reference is labeled by dash line again, and the reactivity of IDSRRs is denoted by clear circles. (b) Measured transmission characteristics of IDSRRs and reference response at 50 degree incident. The reference is presented by dash line; the result of pure IDSRRs is shown by bold solid line.

The next step needs to proceed should be implying such IDSRR pattern for the DRF design and measuring the response. The final target is to get a practical solution for the power insufficiency of metamaterials.

4.3.2 Design for DRF-DSRR Basing on IDSRR

The overall schematic layout of DRF-DSRR basing on IDSRR is shown, where black area consists of copper, and white part is excavated by engraving machine. Lattice constant of large DSRR is still 60mm while that of small DSRR changes to 5mm according to prior experiment data. 60mm, the lattice constant of large one, is chosen by calculation. Meanwhile, 20 units of small DSRRs are removed from each large DSRR pattern. Basically, the only difference between large and small DSRRs is the scale; large DSRR can be viewed as the magnified pattern of small one. That is, the linewidths are 7.86mm and 0.655mm separately. The relative position between large and small DSRRs is depicted clearly in Fig. 4.13. A large DSRR is divided into four parts, and the exactly position is labeled by the unit of millimeter in the schemes either.

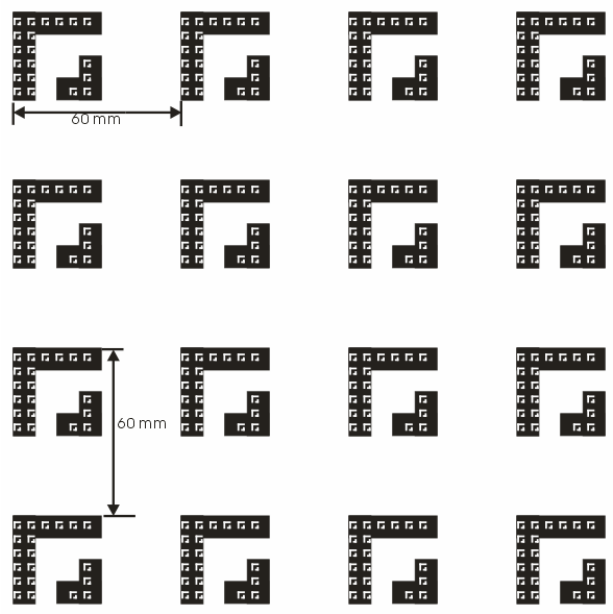

Figure 4.12: Overall schematic layout for DRF-DSRR basing on IDSRR. Each lager DSRR consists of 20 small engraved DSRRs. The lattice constant of large DSRRs is set to be 60mm while the lattice constant of small ones is 5mm. Meanwhile, the linewidth of large DSRR is 7.86mm, and that of small one is 0.655mm.

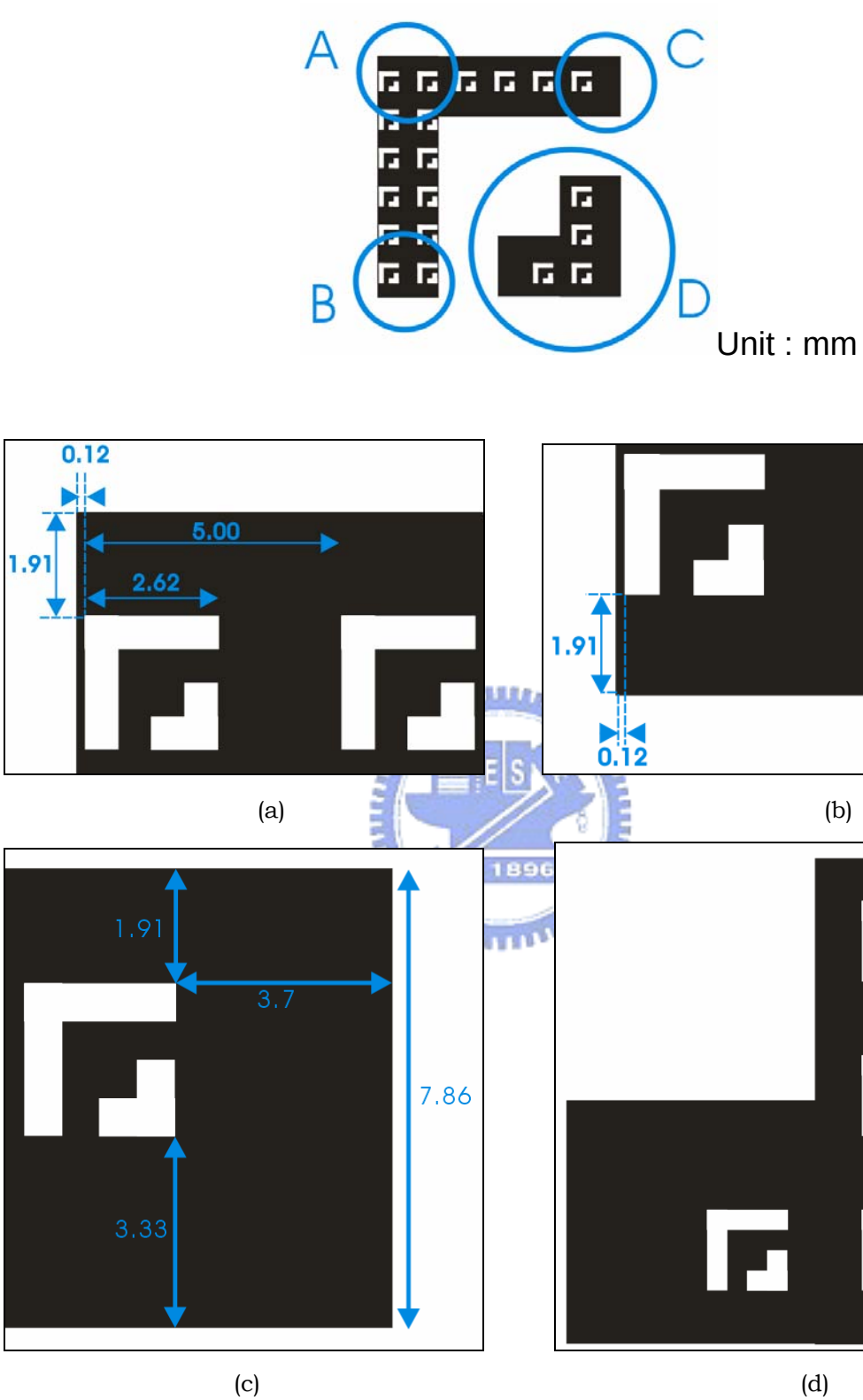

Figure 4.13: Relative position between large and small DSRRs. A large DSRR unit is shown first, and zoom in areas are illustrated in (a), (b), (c), and (d) respectively.

In the following experiment verification, two different frequency ranges will be measured around 1GHz and 15GHz respectively. The experiment procedure will begin from the measurement at high frequency spectrum first; a single PCB contains 16 unit metallic cells is used. We are hoping that the absorption phenomenon will still maintain for higher spectrum detection, of course, at the degree other than 90, so that it can be used to retrieve power loss of metamaterials. As for the low frequency detection, the pattern used for this experiment comprised of 12 pieces of the pattern shown in Fig. 4.12. In other words, a pattern with total 192 large DSRRs will be under investigated when all facilities are exactly identical to that mentioned in Sec. 4.2.2.

4.3.3 Experiment Verification

High Frequency Response

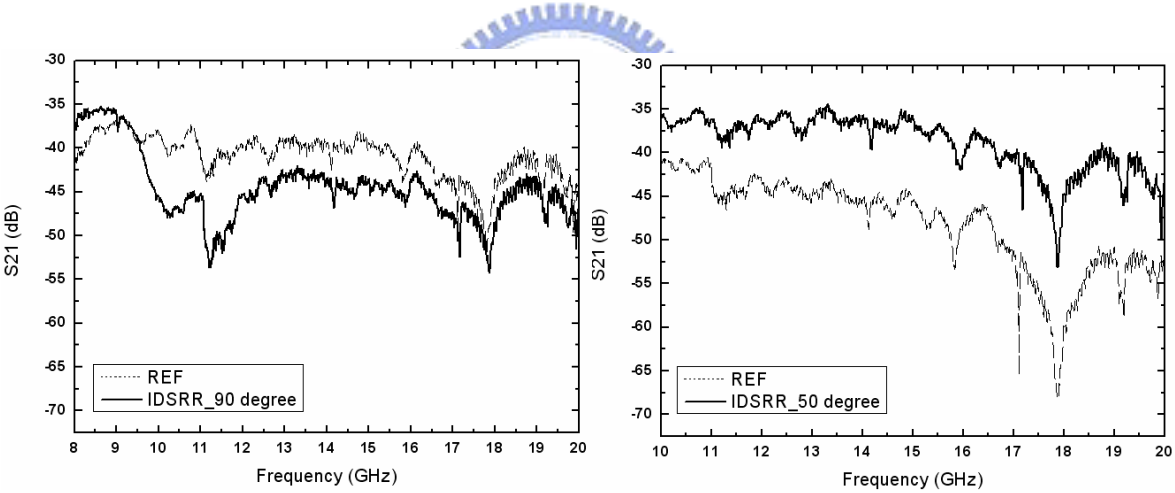

(a) (b)

Figure 4.14: (a) The spectrum of DRF-DSRR basing on IDSRR at 90 degree. The reference is labeled by dash line, and the reactivity of IDSRRs is denoted by bold solid line. (b) Measured transmission characteristics of IDSRRs whose label is identical to (a) except for 50 degree incident.

The response of DRF-DSRR basing on IDSRR begins from the discussion at 90 degree incident that was barely inactive in pre-experiment. As shown in Fig. 4.14 (a),

the interaction between sample and external microwaves is distinguished from that in pre-experiment; slight absorption extends from 9.50GHz to 18GHz. The inapparent power drop, of course, is not caused by the negative permeability since the estimated resonant frequency of large DSRRs should locate at low frequency spectrum such as 1GHz. Hence the phenomenon must be introduced by another mechanism. In fact, the metal parts which are divided by engraved small DSRRs remind us the similar existence of cut wires [16]. Just like the orderly layout of discontinuous wires mentioned in Ch.3, metallic area shown in Fig. 4.12 which distributes irregularly has stop-band characteristics similar to cut wires. In other words, the reason why the absorption phenomenon appears is actually the effect of negative permittivity.

Next, the most expected response is the response of DRF-DSRR basing on IDSRR at 50 degree. However, its final results display a total different activity from that in pre-experiment. Instead of showing an obvious absorption around 16GHz, the spectrum curve of 50 degree incident imitates the curve of reference sample despite a power shift about 10dB. As shown in Fig. 4.14 (b), the response of patterns has higher transmission scattering parameter S21 than that of reference sample. If the metal area of these two samples is included for consideration, then it is extremely easy to explain the phenomenon. The area covered by metal of DRF-DSRR sample shown in Fig. 4.12 is not over 17% which is far below the 100% ratio of reference sample. Hence, the microwave can easily pass through the DRF-DSRR pattern at 50degree incident while it will be reflected by the reference sample at the same degree.

Low Frequency Response

After discussing the experiment data at X-band, the response at low frequency region is illustrated in Fig. 4.15. The pattern comprises of 16x12 large DSRR cells is placed parallel to the propagating direction of the incident waves, where the magnetic field penetrates all metallic structures. Again, the activity of free space without any sample in the middle of two horn antennas is denoted by solid squares when the expected response of DRF-DSRR is labeled by clear triangles. Apparently, the curves of free reference and DRF-DSRR pattern do not have significant dissimilarity. The

maximum difference between them is extremely small if the absorption level at higher band about several decades observed is taken as the standard. The difference, not over 2.5dB, might be thought as inevitable noise fluctuation of whole system instead of any meaningful physical reaction.

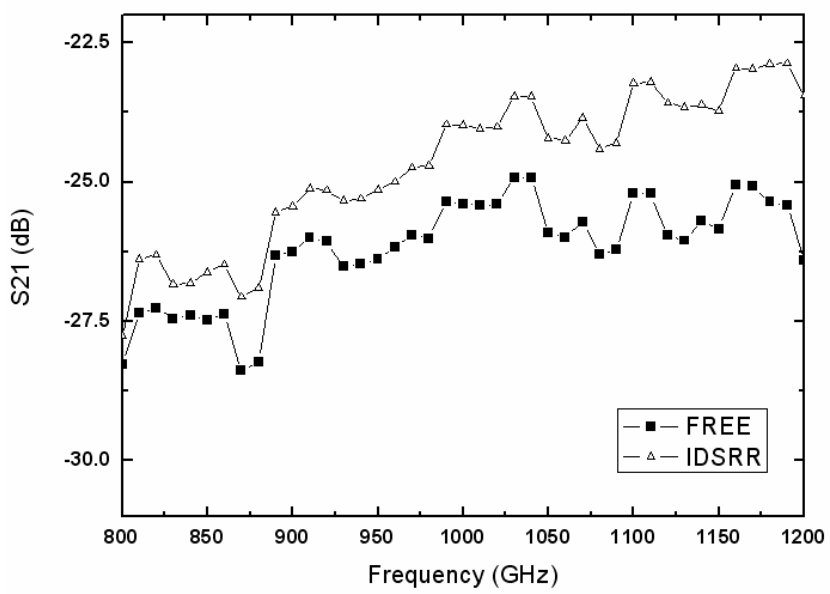

Figure 4.15: Final experiment results of DRF-DSRR pattern basing on IDSRR at lower band when the propagating direction is parallel to the PCB. Solid squares denotes the response of free space, and clear triangles indicates the reactivity of a 16x12 large DSRR array whose lattice constant is 60mm.

4.3.4 Summary

In summary, the behavior of DRF-DSRR basing of fractal-like IDSRR only achieves a part of the estimated approaches eventually. In contrast to the positive experiment results in pre-experiment, all the information obtained for DRF-DSRR basing on IDSRR totally differ from foregoing evaluations. Disparate response for DRF-DSRR basing on IDSRR at high frequency spectrum comparing to that in pre-experiment delivers a hint of failure for the following procedure, and the flat curve at low frequency range negates the existence of double resonant frequency pattern in the end.

Generally, a negative prediction can be made through comparing the different experiment results between DRF-DSRR and the pattern in pre-experiment. Obvious transmission dropping curve appears around 16GHz at 50 degree for the pattern shown in Fig. 4.10 while the interaction between DRF-DSRR is almost inactive. The crucial factor that introduces the divergent behaviors is the schematic layout. For the pattern in pre-experiment, all inverse DSRRs are excavated regularly in a square architecture so that the S21 parameter has a sharp drop at 50 degree. Nevertheless, the small DSRRs will not construct a square scheme anymore when they are engraved only within the region of large metallic DSRRs. In this situation, the DRF-DSRR sample does not have any response to the incident electromagnetic waves. Hence the power drop at 50 degree for pre-experiment sample might be the effect of reflection instead of the expected absorption. If this conclusion is truly right, then it is impossible to utilize such a mechanism to compensate the power loss of meta -materials whether the final experiment results at low frequency spectrum are successful.

4.4 Discussion and Conclusions

In the process of seeking key points for counterpoising the power insufficiency of meta -materials, two methods of SDSRR and IDSRR endeavor to solve this problem. All the procedures from sample design to practical experiment are depicted in Sec.4.2 and Sec.4.3 respectively.

Basing on the concept of SDSRR, there is still a great chance applying such a mechanism to compensate the power loss although direct evidence is not yet available. An over loosen structure of DRF-DSRR may prohibit the generation of flowing currents on the surface of metallic DSRRs, thus a high density of DRF-DSRR structure (more small DSRR cells in per large DSRR cell) is necessary for further demonstration. Now, a DRF-DSRR sample is going to be fabricated through semiconductor process; its resonant frequencies will locate at X-band and 1550nm infrared region by considering the limitation of existing facilities. The behavior of this sample at X-band will provide sufficient facts that determine whether the idea of SDSRR is useful or not. Moreover, if it works, the cooperative response of

microwaves and infrared light on the same piece of sample is worthy for studying as well. The intrigued interaction may inspire additional inspirations in the future.

As for the idea of IDSRR, the experiment data of DRF-DSRR basing on IDSRR have claimed the failure for counterpoising power loss of metamaterials. The inverse DSRRs can only induce reflection effects while they are placed regularly at certain angle. When small DSRRs change to sporadic formation, this phenomenon would not exist anymore and is useless for predicted purpose. Therefore, applying IDSRR on DRF-DSRR is not a realistic method to reach our target in this chapter. The experiment data indicate the possibility of implementing IDSRR for DRF-DSRR approaches to zero.

Chapter 5

Optical Response of Metamaterials

In the previous two chapters, the operating frequency is about several GHz, and all patterns are designed under the restriction of X-band. The ultimate destination, however, is realizing metamaterials for modern optical system. Hence, samples and their response corresponding to extremely high frequency (about tera-hertz) are important for this study. In this chapter, some metamaterials samples provided by Industrial Technology Research Institute (ITRI), including DSRRs and metallic wires, will be investigated in optical spectrum. The experiment results will be analyzed and compared with theoretic assumptions to see if there is any possibility for the accomplishment of metamaterials within infrared region.

5.1 Experiment Setup

The optical experiment setup is a little different from the microwave one. A tunable laser (Agilent, 81682A Tunable Laser Module; operating frequency range is from 1400-1580 nm) connecting to a power amplifier (Erbium-Doped Fiber Amplifier, 1530nm to 1562nm) with 22dB gain is used to produce coherent and steady light source with essential power as shown in Fig. 5.1 (a). After magnified by EDFA, the output light is connected through an optical fiber with a fiber pigtail. A set of lens following the fiber pigtail is used to collimate the divergent source so it would almost

tend to be plane waves after passing the lens set. At this time, the beam diameter of the operating light is 4mm.

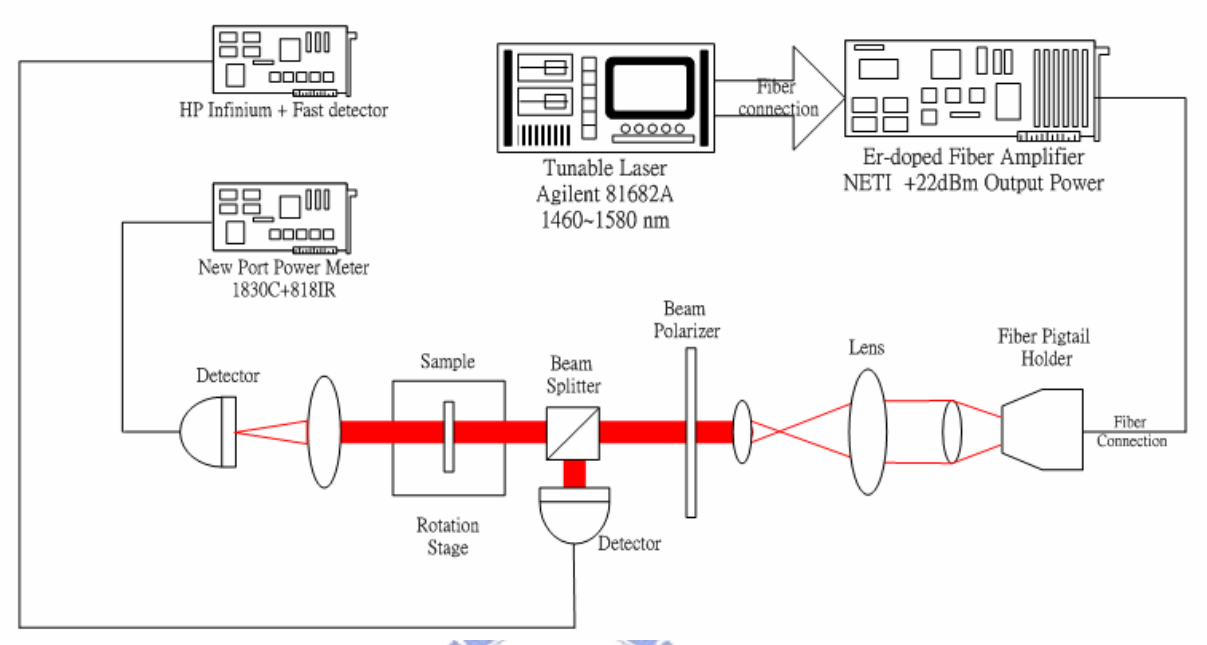

(a)

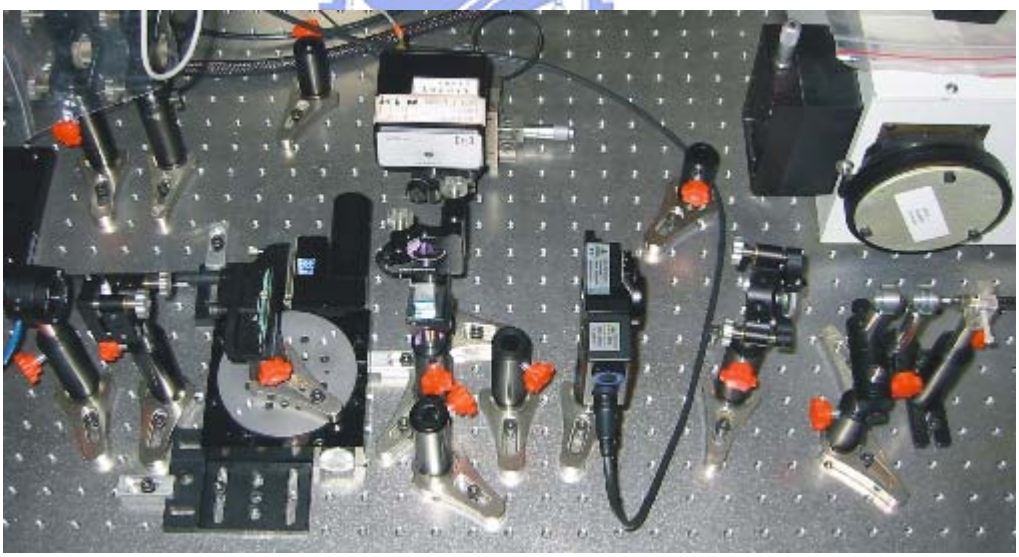

(b)

Figure 5.1: (a) Top view of the experiment Setup for infrared region. The angle is set to be 0 while the sample is perpendicular to the incident light. (b) Photograph of practical experiment setup.

Next, in order to force the electric field coinciding with the desired direction (perpendicular to the optical table), a polarizer is introduced on the optical path. A beam splitter following the polarizer can separate the source into two parts. One is taken as the monitoring light for reference, and another one is propagating directly into the sample. Meanwhile, two sets of detectors and powermeters (Newport, 1830-C Optical Power Meter with 818 IR detector; HP, Infinium Oscilloscope with Newfocus 1611 High-Speed Photoreceiver) are applied in this experiment for simultaneously detection. For the observed sample, a rotation stage (Newport, ESP 300 Motion Controller/Drive with VP-25XA Precision Compact Linear Stage) is constructed under the sample to change the relative angle between incident light and our pattern. The rotation angle is set to zero when the incident light is perpendicular to the sample surface. During the experiment process, the angle will start rotation from 80 to 100 degree. Behind the sample, a lens is used to collect light beam to prevent any diffraction phenomenon.

5.2 Sample Specification

Before start descriptions of the design details about our samples, the issue concerning manufacture should be emphasized first because conventional process may not meet our request. In a standard semiconductor process, the most common material is silicon. Such a material will introduce about 50% significant reflection while it was applied at infrared band, which may reflect most of the incident beam before it encounters the patterns. Then it is totally impossible for the pattern to interact with the electromagnetic waves at all. Moreover, heavy reflection will also cause heavy power loss besides the intrinsic metamaterials properties, and the power efficiency will be more difficult to solve. Due to the requirement of substrate material, another material which has minute reflection would be the best choice. Fortunately, cooperative ITRI group has invented a new fabricating process consisting of nano-imprinting and lift-off techniques [19] so that the substrate can be made by acrylic polymer which is transparent and subtle reflecting for 1550nm. Thus all samples in this experiment will be constructed on the acrylic substrate in the following sections. Furthermore, acrylic substrate is convenient except for preventing

significant power loss in the optical system when it is combined with other optical components, such as lens, in the future.

5.2.1 DSRR pattern

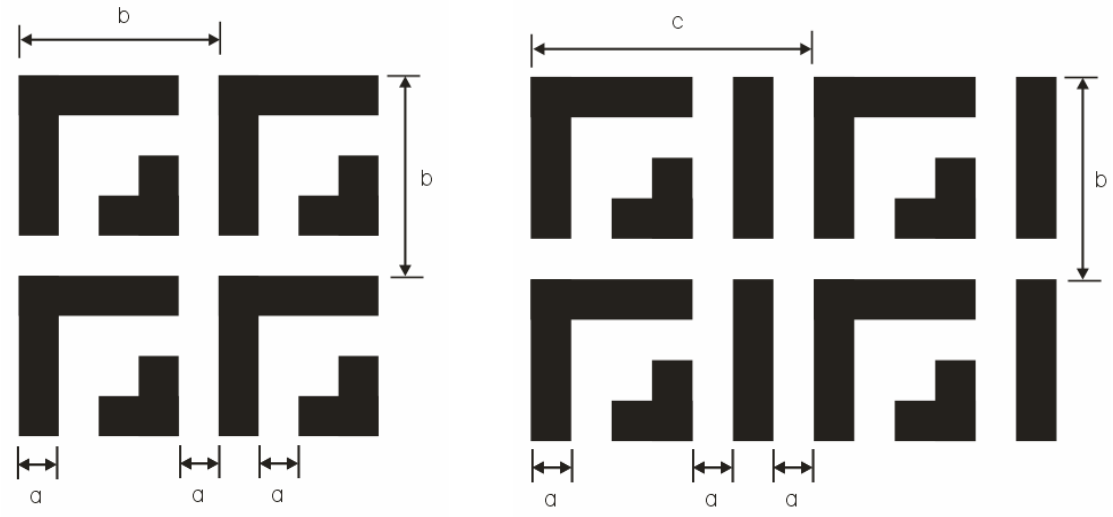

(a) (b)

Figure 5.2: (a) Schematic layout of DSRR pattern. Linewidth *a* is equal to 0.2um while lattice constant *b* is 1.0um. (b) The structure of DSRRs with cut wires whose linewidth is also 0.2um. By inserting discontinuous wires between two DSRRs, the lateral lattice constant *c* changes to 1.4um.

The design of DSRRs at 1550nm is similar to that at X-band except for extremely small scale, pattern metal and different substrate. As shown in Fig. 5.2, DSRR pattern and DSRRs with cut wires are illustrated clearly. All of the linewidth and intervals are equal to *a*, which is solely 0.2um therefore the lattice constant in Fig. 5.2 (a) is just 1.0um. In contrast to the identical lattice dimension in both directions for DSRRs alone, the lateral lattice constant of Fig. 5.3 (b) has a little modification. Cut wires are inserted in the middle of two DSRRs and for this reason the lattice constant will increase from 1.0um to 1.4um. Finally, completed DSRR and wire cells are presented in Fig. 5.3 through SEM. All structures are made by gold, and its thickness does not exceed 100nm. The total pattern area of each sample is $2 \times 2\ mm^2$, and the substrate size is $4 \times 4\ mm^2$ while its thickness is 3mm.

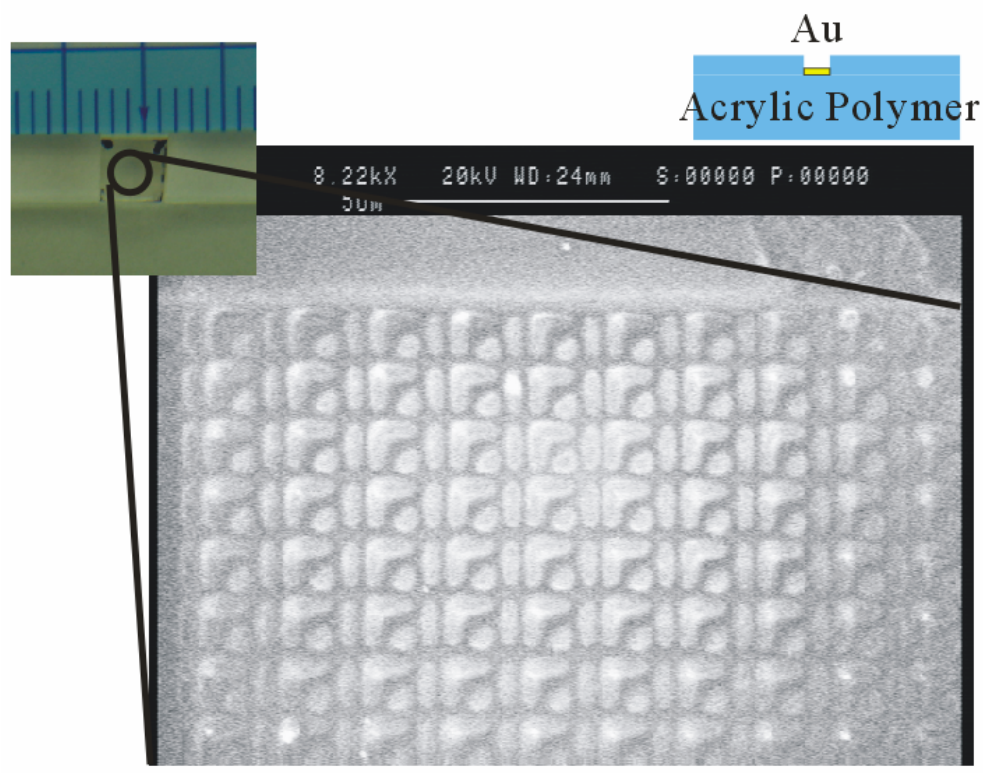

Figure 5.3: SEM Photograph of DSRRs and wires. All DSRRs and wires are fabricated by gold, and the substrate is acrylic polymer.

5.2.2 Metallic Wire Line Grating Pattern

The specification of metallic wire line grating pattern is depicted in Fig. 5.4 (a). The width w of linewidth and the spacing between two lines are both 80nm, which implies 40nm wire radius and 160nm lattice constant. The area covered by metallic wires is $40 \times 40\ mm^2$, thus the wire length L is 40mm. Meanwhile, the material used for wires is aluminum while the substrate is glass. Fig. 5.4 (b) shows photographic image of the whole sample. Some external glue is adhered on the plate, but it does not affect the experiment results since light will not pass those polluted areas.

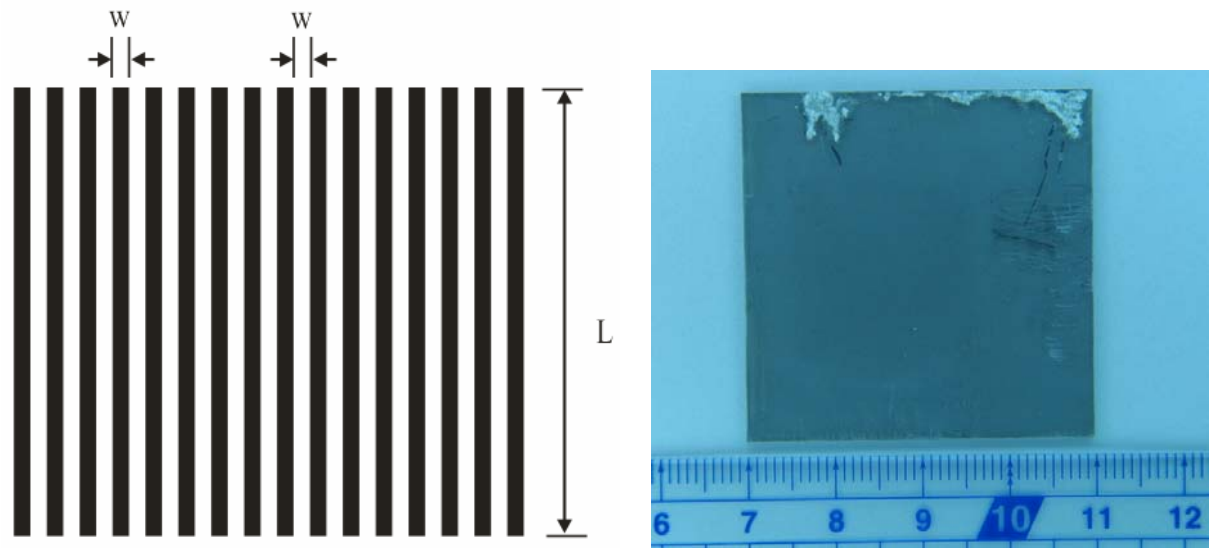

(a) (b)

Figure 5.4: (a) Schematic layout of metallic wire ling grating. Linewidth w is equal to 80nm while lattice constant 160nm. The wire length L is 40mm. (b) Photograph of practical sample whose width and length are both 40mm.

5.3 Experiment Results

5.3.1 DSRR Pattern

The experiment results of nano-scale DSRR pattern now is shown in Fig. 5.5. The experiment starts from 80 degree incident to 100 degree, and the resolution is 0.1 degree. The response of two samples, DSRRs alone and DSRRs with discontinuous wires, are presented together to make an easy comparison. The transmission power of DSRRs increases as the angle increasing from 80 to 90 degree. The power reaches its peak value, 1.37mW, while the rotation angle is 88.3 degree. After the maximum power transmission, the curve starts to decrease while the rotation angle continues to move. The behavior of the whole pattern shows there in no absorption phenomenon at all. If the DSRRs actually bring the effect of negative permeability, then significant absorption is supposed to occur around 90 degree just as what we observed in previous chapters. However, the experiment data gives the evidence that there is neither any power drop nor the activity of negative permeability.

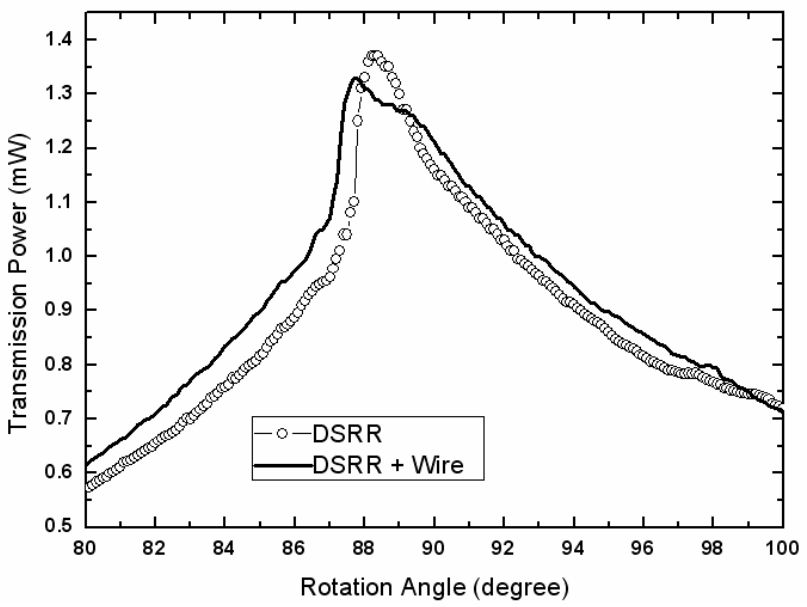

Figure 5.5: Measured transmission power of nano-scale DSRR sample. The response of DSRRs alone is marked by clear circles while the activity of DSRRs with wires is denoted by bold solid line.

Since there is barely response for the DSRR alone, then the transmission curve of DSRRs and wires is supposed to be inactive either. According to the experiment data shown in Fig. 5.5, the pattern of DSRRs and wires has a smooth curve similar to a blank sample. In fact, both responses of DSRRs alone and composite DSRRs are almost identical despite of subtle difference at the peak position. Generally, the uneven faces which are cut manually will introduce uncertainties in the experiment; including the position of transmission peak. Therefore, the similar curve may be caused by the intrinsic property of acrylic substrate itself, which the incident light will have maximum transmission power when the substrate plate is parallel to the beam. In other words, the predicted absorption of negative permeability does not happen eventually.

5.3.2 Metallic Wire Line Grating Pattern

The measurement optical response of metallic wire line grating pattern is shown in Fig. 5.6 as rotating from 80 to 100 degree with the resolution is 0.1 degree. By

viewing the experiment data, the estimated absorption while the incident beam is parallel the periodic wires does not happen. Instead of that, a strong transmission, whose peak value is 6.69mW, occurs in the range from 91 to 93 degree. On the other hand, the power measured at remaining degrees is extremely minute because of the heavy reflection of the sample itself. The light source passes the sample only when it is almost parallel to the sample plane, where smallest reflection occurs. Therefore, the curve of our metallic periodic sample without any absorption is simply the activity of a single opaque plate. Comparing to the smooth curve in Fig. 5.5 due to transparent acrylic substrate, the sharp curve in Fig. 5.6 is caused by the heavy reflection of the metallic substrate. Otherwise, a power drop is supposed to happen while the incident wave encounters numerous metallic periodic wires in the propagating direction.

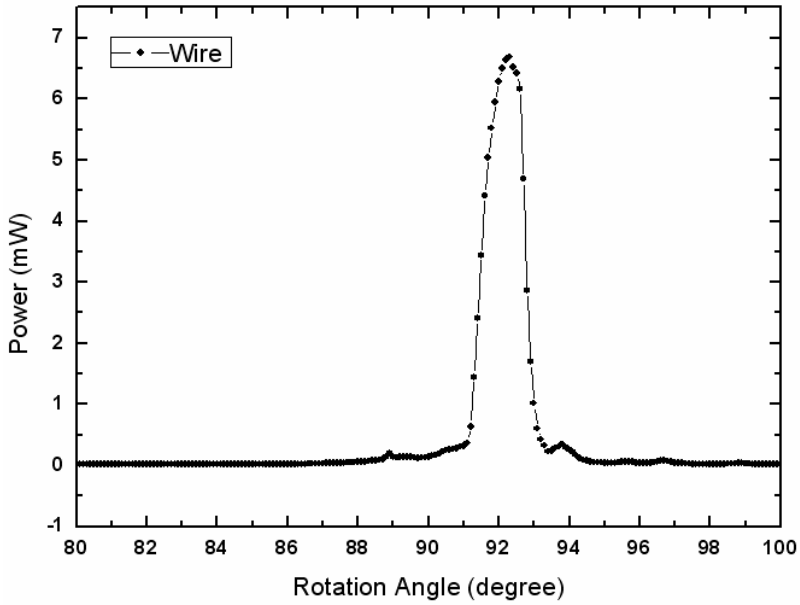

Figure 5.6: Measured transmission power of nano-scale metallic wire structure from 80 to 100 degree.

5.4 Discussion and Conclusion

According the experiment results mentioned above, we can conclude that neither DSRR pattern nor wire structure has the predicted response. The reason why they can

not achieve the target of negative property can be discussed in details below.

First we start to figure out the failure factors of DSRR sample itself. Due to prior knowledge, the lattice constant of DSRRs should be 1/6 of operating wavelength; that is, absorption only happens while the lattice constant is around 1/6 of the resonant frequency. In this experiment, operating wavelength is 1550nm thus the lattice constant of effective DSRR pattern should be about 258nm, which is much smaller than 1um. The absorption does not occur in this experiment since the resonant phenomenon is supposed to appear at lower frequency (longer wavelength). In fact, the corresponding resonant frequency of a DSRR pattern with 1um lattice constant is 5×10^{13} Hz (6um operating wavelength) results the power drop not appearing. Furthermore, another factor, the total number of cells, should be included for concern as well. On the surface of a DSRR sample, there are totally 4×10^{6} cells in the $2\times2\ mm^{2}$ area. The relation of resonant frequency and the total number of cells reminds us that the resonant frequency of nano-scale DSRR pattern will shift significantly to lower frequency again (longer wavelength), thus it even pushes the resonant toward the spectrum lower than 5×10^{13} Hz. In summary, two main factors that control the position of resonant frequency both show the intendancy of frequency shifting towards lower spectrum. For seeking the presentation of negative permeability, a light source with larger wavelength should be used to obtain the desired experiment results.

As for the metallic wire line grating sample, some formulas should be reviewed first. In the process of developing the estimation of plasma cutoff frequency of metallic wires, there are actually three different assumptions. One has been mentioned in Eq.3.1. Here all of them are listed below.

$$\texttt{Pendry:}\quad f_p^{\,2}=\frac{c_{light}^{\,2}}{2\pi a^2\ln(a/r)} \tag{5.1}$$

$$\texttt{Sarychev:}\quad f_p^{\,2}=\frac{c_{light}^{\,2}}{2\pi a^2\left[\ln(\frac{a}{\sqrt{2}\,r})+\frac{\pi}{2}-3\right]} \tag{5.2}$$

$$\text{Maslovski:}\quad f_p^{\,2} = \frac{c_{light}^{\,2}}{2\pi a^2 \ln\left[\dfrac{a^2}{4r(a-r)}\right]} \tag{5.3}$$

where f_p is the plasma frequency, a is the lattice constant, r is the wire radius and c_{light} is the speed of light in vacuum. For the metallic wire sample, a = 160nm and r = 40nm. If these parameters are replaced into Eq.5.1 to Eq5.3 and Eq.3.2, then the effective permittivity, the plasma frequency and its corresponding wavelength could be obtained in table 5.1.

Table 5.1: Calculation effective permittivity and plasma frequency through three different formulas

	Linewidth (nm)	f_p(Hz)	λ_p(nm)	ε_{eff}
Pendry	80	6.35×10^{14}	472.21	-9.77
Sarychev	80	NA	NA	NA
Maslovski	80	14.95×10^{14}	215.12	-50.72

As shown in the table, two of the three formulas give the plasma frequency far above the operating one (1550nm, 1.94×10^{14} Hz), which means the metallic structure can present negative permittivity property in the experiment. Also, the effective value of permittivity is shown in the table. However, the plasma frequency by calculating through Eq.5.2 is not available because close ratio of lattice constant to wire radius gives negative value of Eq.5.2, and the plasma frequency becomes imaginary. Thus it is impossible for such a metallic structure to have the character of negative permittivity in Sarychev's estimation

By introducing the experiment data and comparing them to the calculation data, the one computed through Eq.5.2 is most practical since there is no absorption around 90 degree in the realistic measurement. The experiment data demonstrate Sarychev's

estimation is the most precise formula for calculating the plasma frequency of metallic wires. In fact, the accuracy of Sarychev's deduction comes from its consideration of varied potential vector which is assumed to be constant in Pendry's and Maslovski's concept. By introducing the R-dependent potential vector [20], the effective permittivity will change thus the square of plasma frequency with a factor will be obtained through replacing $\ln(a/r)$ in Eq.5.1 by $\ln(\frac{a}{\sqrt{2}r})+\frac{\pi}{2}-3$. In such an equation, the ratio of lattice constant to wire radius must not exceed 5.9 to ensure the existence of plasma frequency and negative permittivity.

In conclusion, the experiment results of DSRR and wire samples do exhibit neither negative permeability nor negative permittivity characteristics in optical spectrum. More samples matching the requests are necessary for advanced demonstration.

Chapter 6

Conclusion and Future Work

6.1 Conclusion

Except for fundamental knowledge introduced in chapter 2, two main topics are discussed through a series of design, experiment data and simulation results in this thesis.

A coplanar structure consisting of symmetric DSRRs and discontinuous wires is purposed for advanced manufacturing semiconductor process. The ultimate destination for this coplanar sample is fabricating metamaterials on a single plane which can solve alignment problem since it is extremely difficult for such a small scale. The experiment results shows that symmetric DSRRs, wire1, wire2, and wire3 do have their own predicted properties such as negative permeability and permittivity property separately while the cut wire4 has some kind of gratting character out of prior assumption. If symmetric DSRRs and short wires are put together, the original trait of wires will be covered by the property of ring structure. On the contrary, the wire structure will dominate the character of whole pattern when symmetric DSRRs is combined with wire4, the longest wire. Therefore, the idea of implementing a single symmetric DSRR and wire to build up metamaterials in an independent cell is not applicable although they do have their estimated features seperately.

In chapter 4, two different mechanisms, split DSRR and inverse DSRR, are used to construct DRF pattern for compensating power consumption. Some preliminary

experiment data indicate that there is still a great chance for the first mechanism, SDSRR, to reach the target of DRF. The fractal-like SDSRRs can also have a high frequency resonant even when they are not placed regularly in a square layout. Some patterns through semiconductor process are going to be fabricated now; more clearly conclusions can be made after obtaining further experiment data. In contrast to the positive results for SDSRR, the second mechanism, IDSRR, gives negative conclusion. A series data gathered from different samples demonstrates excavated small DSRRs only showing some reflection effects at 50 degree, and in the schematic array formation. The feature of them is not benefit at all because they are designed for counterpoising transmission power originally.

6.2 Future Work

There are two available research directions extending from our present work:

- DRF-DSRR basing on SDSRR. As mentioned in chapter 4, the chance for accomplishing a power compensating metamaterials by SDSRRs is highly estimated. Its resonant frequency regions are set for X-band and infrared. If it does has response at X-band, then myriad applications is applicable.
- Metallic wires in infrared region. For the technique of modern semiconductor process, it is not difficult to manufacture a metallic wire structure whose permittivity is negative at infrared region such as 1550nm. A sample with $a/r \geq 6$ such as 100nm linewidth with lattice constant of 300nm or 400nm can approach our target without extremely difficulties.

Bibliography

[1] V. G. Veselage, “The Electrodynamics of Substances with Simultaneously Negative Values of ε and μ,” Sov. Phys.-Usp. **10,** 509 (1968).

[2] http://www.darpa.mil/dso/thrust/matdev/metamaterials/program.html

[3] J. B. Pendry, A. J. Holden, D. J. Robbins, and W. J. Stewart, “Magnetism from Conductors and Enhanced Nonlinear Phenomena,” IEEE Trans. Microwave Theory Tech. **47**, 2075 (1999).

[4] R. A. Shelby, D. R. Smith, and S. Schultz, “Experimental Verification of a Negative Index of Refraction”, Science **292**, 77 (2001).

[5] R. A. Shelby, D. R. Smith, S. C. Nemat-Nasser, and S. Schultz, “Microwave Transmission through a Two-Dimensional, Isotropic, Left-Handed Metamaterial,” Appl. Phys. Lett. **78,** 489 (2001)

[6] J. B. Pendry, “Negative Refraction Makes a Perfect Lens,” Phys. Rev. Lett. **8**5, 3966 (2000)

[7] J. B. Pendry, A. J. Holden, W. J. Stewart, and I. Youngs, “Extremely Low Frequency Plasmons in Metallic Mesostructures,” Phys. Rev. Lett. **76**, 4773 (1996)

[8] J. B. Pendry, A. J. Holden, D. J. Robbins, and W. J. Stewart, “Low Frequency Plasmons in Thin-Wire Structures,” J. Phys. : Condens. Matter **10**, 4785 (1998)

[9] D. R. Smith, W. J. Padilla, D. C. Vier, S. C. Nemat-Nasser, and S. Schultz, “Composite Medium with Simultaneously Negative Permeability and Permitvitty,” Phys. Rev. Lett. **84,** 4184 (2000)

[10] Y. C. Huang, Y. J. Hsu, J. S. Lih, and J. L. Chern, “Transmission Characteristics of Deformed Split-Ring Resonators,” Jap. J. Appl. Phys. **43**, L190 (2004)

[11] Y. C. Huang, Y. C. Huang, J. S. Lih, and J. L. Chern, “Electromagnetic resonance in deformed split ring resonators of left-handed meta-materials,” J. Appl. Phys. **96**, 1979 (2004)

[12] E. Ozbay, K. Aydin, E. Cubukcu, and M. Bayindir, “Transmission and Reflection Properties of Composite Double Negative Metamaterial in Free Space,” IEEE Trans. Antennas Propagation **51**, 2592 (2003)

[13] B. B. Mandelbrot, “The Fractal Geometry of Nature,” W. H. Freeman and Company, 1983

[14] K. Falconer, “Fractal Geometry – Mathematical Foundations and Applications,” Wiley, 1990

[15] P. Markos, and C. M. Soukoulis, “Absorption Losses in Periodic Arrays of Thin Metallic Wires,” Op. Lett. **28**, 846 (2003)

[16] T. Koschny, M. Kafesaki, E. N. Economou, and C. M. Soukoulis, “Effective Medium Theory of Left-Handed Materials,” Phys. Rev. Lett. **93**, 107402-1 (2004)

[17] Y. J. Hsu and J. L. Chern, “Transmission Characteristics of Smiling Pattern Resonators,” Jap. J. Appl. Phys. **43**, L669 (2004)

[18] J. S. Lih, Y. S. Wang, M. C. Lu, Y. C. Huang, K. H. Chen, J. L. Chern, and L. E. Li, “Experimental Realization of Breaking Diffraction Limit by Planar Negative-Index Metamaterials in Free Space,” Europhys. **69**, 544 (2005)

[19] R. Y. Tsai, P. Lai, J. L. Chern, C. S. Chu, “Using Nanolithography and UV Cure Imprinting for Deformed-Split-Ring Resonators Fabrication,” IUMRS-ICA-2004 Paper ID:71

[20] A. K. Sarychev, R. C. McPhedran, V. M. Shalaev, “Electrodynamics of metal-dielectric composites and electromagnetic crystals,” Phys. Rev. B **62**, 8531(2000)